Pathogenic Variants in the Myosin Chaperone UNC-45B Cause Progressive Myopathy with Eccentric Cores

Sandra Donkervoort, Carl Kutzner, Ying Hu, Xavière Lornage, John Rendu, Tanya Stojkovic, Jonathan Baets, Sarah Neuhaus, Jantima Tanboon, Reza Maroofian, et al.

Please cite this article in press as: Donkervoort et al., Pathogenic Variants in the Myosin Chaperone UNC-45B Cause Progressive Myopathy with Eccentric Cores, The American Journal of Human Genetics (2020), https://doi.org/10.1016/j.ajhg.2020.11.002

ARTICLE

Pathogenic Variants in the Myosin Chaperone UNC-45B Cause Progressive Myopathy with Eccentric Cores

Sandra Donkervoort,[1,34] Carl E. Kutzner,[2,3,34] Ying Hu,[1] Xavière Lornage,[4] John Rendu,[5,6] Tanya Stojkovic,[7] Jonathan Baets,[8,9,10] Sarah B. Neuhaus,[1] Jantima Tanboon,[11,12] Reza Maroofian,[13] Véronique Bolduc,[1] Magdalena Mroczek,[14] Stefan Conijn,[15] Nancy L. Kuntz,[16] Ana Töpf,[14] Soledad Monges,[17] Fabiana Lubieniecki,[17] Riley M. McCarty,[1] Katherine R. Chao,[18] Serena Governali,[15] Johann Böhm,[4] Kanokwan Boonyapisit,[19] Edoardo Malfatti,[20] Tumtip Sangruchi,[11] Iren Horkayne-Szakaly,[21] Carola Hedberg-Oldfors,[22] Stephanie Efthymiou,[13] Satoru Noguchi,[12,23] Sarah Djeddi,[4] Aritoshi Iida,[24] Gabriella di Rosa,[25] Chiara Fiorillo,[26,27] Vincenzo Salpietro,[26,27] Niklas Darin,[28] Julien Fauré,[5,6] Henry Houlden,[13] Anders Oldfors,[22] Ichizo Nishino,[12,23,24] Willem de Ridder,[8,9,10] Volker Straub,[14,29] Wojciech Pokrzywa,[30] Jocelyn Laporte,[4] A. Reghan Foley,[1] Norma B. Romero,[7,31,32] Coen Ottenheijm,[15,33] Thorsten Hoppe,[2,3,35,*] and Carsten G. Bönnemann[1,35,*]

Summary

The myosin-directed chaperone UNC-45B is essential for sarcomeric organization and muscle function from *Caenorhabditis elegans* to humans. The pathological impact of UNC-45B in muscle disease remained elusive. We report ten individuals with bi-allelic variants in *UNC45B* who exhibit childhood-onset progressive muscle weakness. We identified a common *UNC45B* variant that acts as a complex hypomorph splice variant. Purified UNC-45B mutants showed changes in folding and solubility. *In situ* localization studies further demonstrated reduced expression of mutant UNC-45B in muscle combined with abnormal localization away from the A-band towards the Z-disk of the sarcomere. The physiological relevance of these observations was investigated in *C. elegans* by transgenic expression of conserved UNC-45 missense variants, which showed impaired myosin binding for one and defective muscle function for three. Together, our results demonstrate that UNC-45B impairment manifests as a chaperonopathy with progressive muscle pathology, which discovers the previously unknown conserved role of UNC-45B in myofibrillar organization.

Introduction

Muscle development and function require a complex system of structural and motor proteins organized into contractile units referred to as sarcomeres. The sarcomeric repeat is a supra-molecular dynamic structure in which actin and myosin filaments, together with associated proteins, are arranged in a precise order. The near crystalline

[1]Neuromuscular and Neurogenetic Disorders of Childhood Section, National Institute of Neurological Disorders and Stroke, National Institutes of Health, Bethesda, MD 20892, USA; [2]Institute for Genetics and Cologne Excellence Cluster on Cellular Stress Responses in Aging-Associated Diseases, University of Cologne, 50931 Cologne, Germany; [3]Center for Molecular Medicine Cologne, University of Cologne, 50931 Cologne, Germany; [4]Institut de Génétique et de Biologie Moléculaire et Cellulaire, INSERM U1258, CNRS UMR7104, Université de Strasbourg, BP 10142, 67404 Illkirch, France; [5]Centre Hospitalier Universitaire de Grenoble Alpes, Biochimie Génétique et Moléculaire, Grenoble 38000, France; [6]Grenoble Institut des Neurosciences-INSERM U1216 UGA, Grenoble 38000, France; [7]Centre de Référence des Maladies Neuromusculaires Nord/Est/Ile de France, Institut de Myologie, GHU La Pitié-Salpêtrière, Sorbonne Université, AP-HP, 75013 Paris, France; [8]Faculty of Medicine, University of Antwerp, 2610 Antwerp, Belgium; [9]Laboratory of Neuromuscular Pathology, Institute Born-Bunge, University of Antwerp, 2610 Antwerp, Belgium; [10]Neuromuscular Reference Centre, Department of Neurology, Antwerp University Hospital, 2650 Antwerp, Belgium; [11]Department of Pathology, Faculty of Medicine, Siriraj Hospital, Mahidol University, 10700 Bangkok, Thailand; [12]Department of Neuromuscular Research, National Institute of Neuroscience, National Center of Neurology and Psychiatry, 187-8502 Tokyo, Japan; [13]Department of Neuromuscular Disorders, University College London Institute of Neurology, Queen Square, London WC1N 3BG, UK; [14]John Walton Muscular Dystrophy Research Centre, Translational and Clinical Research Institute, Newcastle University, Newcastle upon Tyne NE1 3BZ, UK; [15]Department of Physiology, Amsterdam UMC (location VUmc), 1081 HZ Amsterdam, the Netherlands; [16]Department of Neurology, Northwestern University Feinberg School of Medicine, Chicago, IL 60611, USA; [17]Servicio de Neurología y Servicio de Patologia, Hospital de Pediatría Garrahan, C1245 AAM Buenos Aires, Argentina; [18]Center for Mendelian Genomics, Program in Medical and Population Genetics, Broad Institute of MIT and Harvard, Cambridge, MA 02142, USA; [19]Department of Medicine, Faculty of Medicine, Siriraj Hospital, Mahidol, University, 10700 Bangkok, Thailand; [20]Neurology Department, Raymond-Poincaré teaching hospital, centre de référence des maladies neuromusculaires Nord/Est/Ile-de-France, AP-HP, 92380 Garches, France; [21]Joint Pathology Center, Defense Health Agency, Silver Spring, MD 20910, USA; [22]Department of Laboratory Medicine, Sahlgrenska Academy, University of Gothenburg, 405 30 Gothenburg, Sweden; [23]Department of Genome Medicine Development, Medical Genome Center, National Center of Neurology and Psychiatry, 187-8551 Tokyo, Japan; [24]Department of Clinical Genome Analysis, Medical Genome Center, National Center of Neurology and Psychiatry, 187-8551 Tokyo, Japan; [25]Division of Child Neurology and Psychiatry, Department of the Adult and Developmental Age Human Pathology, University of Messina, Messina 98125, Italy; [26]Pediatric Neurology and Muscular Diseases Unit, G. Gaslini Institute, 16147 Genoa, Italy; [27]Department of Neurosciences, Rehabilitation, Ophthalmology, Genetics, Maternal and Child Health, University of Genoa, 16132 Genoa, Italy; [28]Department of Pediatrics, Institute of Clinical Sciences, Sahlgrenska Academy at University of Gothenburg, 41650 Gothenburg, Sweden; [29]Newcastle Hospitals NHS Foundation Trust, Newcastle upon Tyne NE7 7DN, UK; [30]Laboratory of Protein Metabolism in Development and Aging, International Institute of Molecular and Cell Biology, 02-109 Warsaw, Poland; [31]Université Sorbonne, UPMC Univ Paris 06, INSERM UMRS974, CNRS FRE3617, Center for Research in Myology, GH Pitié-Salpêtrière, 75651 Paris, France; [32]Neuromuscular Morphology Unit, Myology Institute, GHU Pitié-Salpêtrière, 75013 Paris, France; [33]Department of Cellular and Molecular Medicine, University of Arizona, Tucson, AZ 85718, USA
[34]These authors contributed equally
[35]These authors contributed equally
*Correspondence: carsten.bonnemann@nih.gov (C.G.B.), thorsten.hoppe@uni-koeln.de (T.H.)
https://doi.org/10.1016/j.ajhg.2020.11.002.

lattice of the sarcomere coordinates actin-myosin cross-bridge cycling, facilitating sarcomere shortening, filament gliding, and muscle contraction. The folding, stability, and organization of sarcomeric proteins into muscle filaments is governed by molecular chaperones.[1] The fundamental importance of chaperones for the development and maintenance of skeletal muscle is underscored by recent studies indicating that chaperone dysfunction is responsible for a distinct subset of hereditary myopathies. These so-called chaperonopathies are characterized by pathogenic variants in genes encoding chaperones and co-chaperones of structural muscle components. For example, loss of the small heat shock protein CRYAB (MIM: 123590) affects folding of the muscle intermediate filament desmin, clinically manifesting as a myofibrillar myopathy known as αB-crystallinopathy.[2] Additional disease mechanisms include impaired homeostasis of chaperone-assisted selective autophagy (CASA) linked to pathogenic variants in the HSP70 co-chaperone *BAG3* (MIM: 603883), clinically manifesting with a progressive myofibrillar myopathy with significant cardiac as well as peripheral nerve pathologies.[3,4] The subsequent identification of variants in *DNAJB6* (MIM: 611332) that cause limb-girdle muscular dystrophy (LGMDD1) provided clear evidence of abnormal sarcomeric aggregate pathology in these chaperonopathies.[5,6] The clinical spectrum of chaperonopathies has expanded over the last years to include hereditary motor neuropathies, with or without muscle involvement, caused by *HSPB1* (MIM: 602195), *HSPB3* (MIM: 604624), *HSPB8* (MIM: 608014), and *DNAJB2* (MIM: 604139) defects.[7] These examples suggest that abnormal chaperone function is an important driver in neuromuscular disease, suggesting that its correction might be a valid therapeutic approach.[8]

The abovementioned chaperones are involved in the proper folding and stability of aggregation-prone proteins in various cell types, including muscle. In contrast to the broad functional spectrum of many molecular chaperones, more specialized chaperone systems regulate muscle contraction by folding and assembling of conventional type II myosin.[9] Type II myosins are composed of two myosin heavy chains, each containing an identical myosin head, whose folding requires precise temporal and spatial control, mediated by conserved UCS (UNC-45/CRO1/She4p) domain-containing proteins.[10–12] As one founding member of the UCS family, UNC-45 (MIM: 611220) was first identified in *C. elegans*, revealing that conditional loss-of-function mutations result in abnormal myofilament assembly and *uncoordinated* locomotion defects.[13] UNC-45 orthologs exist in all vertebrates, and various point mutations have been associated with skeletal and cardiac function in *C. elegans*, *Drosophila*, zebrafish, and *Xenopus*.[14,15] UNC-45 contains four domains: an N-terminal TPR domain (TPR repeat 1–3), a conserved central domain (ARM repeat 4–5), a neck domain (ARM repeat 6–9), and a C-terminal UCS domain (ARM repeat 10–17) (Figure 1A).[16,17] The N-terminal TPR domain is important for binding to the chaperones Hsp70 and Hsp90, while the C-terminal UCS domain associates with the head of muscle myosin.[18] Mechanistically, UNC-45 oligomers have been described to serve as a multi-site-docking platform, which supports precisely defined collaboration with the general chaperones Hsp70 and Hsp90 in folding and assembly of myosin filaments.[17] Thus, UNC-45 provides substrate specificity for the partner chaperones during late stages of myofibrillogenesis (Figure 1B). The repetitive arrangement of UNC-45 oligomers with myosin-binding UCS domains protruding from the linear protein chain serves as a template that defines the periodicity of myosin organization in growing sarcomeres.

The muscle sarcomere is a complex structure permanently challenged by mechanical stress, which presupposes the dynamic coordination between protein folding and degradation pathways.[1,18] On the basis of its central role as a myosin-directed chaperone, both UNC-45 stability and localization are precisely regulated. UNC-45 degradation is mediated by ubiquitin-dependent proteolysis, which coordinates myosin folding and assembly both in *C. elegans* and human myoblasts.[18,19] Conclusively, defective degradation of UNC-45B in individuals with *VCP*-related inclusion-body myopathy (MIM: 601023) is linked to disorganized myofibrils and impaired sarcomeric function.[19]

Despite the conserved role in myofibrillogenesis and evidence from multiple model organisms, the relevance of muscle-specific UNC-45B dysfunction for the pathology and pathogenesis of human myopathies had remained unclear.[19] Here, we present comprehensive findings that establish bi-allelic pathogenic variants in *UNC45B* (MIM: 611220) as an underlying cause of a chaperonopathy, clinically manifesting as a progressive myopathy with recognizable muscle eccentric core histology in humans.

Material and Methods

Recruitment and Sample Collection

Individuals were identified through their local neurology and genetics clinics. P3 and P4 were identified through GeneMatcher.[20] Written informed consent and age-appropriate assent for study procedures were obtained by a qualified investigator [protocol 12-N-0095 approved by the National Institute of Neurological Disorders and Stroke, National Institutes of Health Institutional Review Board (IRB); project ID: 07/N018, Research Ethics Committee (REC) Ref: 07/Q0512/26 approved by the UCLH local institutional IRB; Protocol 317-05 approved by the Regional Ethical Review Board in Gothenburg (317-05)]. Medical history was obtained and clinical evaluations, including muscle magnetic resonance (MR) imaging and muscle biopsy, were performed as part of the standard diagnostic examination. Muscle MR imaging included T1 axial images of the lower extremities. Muscle biopsy histology slides and electron microscopy (EM) images were independently reviewed. DNA was obtained according to standard procedures.

Whole-Exome and RNA Sequencing

Whole-exome sequencing (WES) was pursued by six independent teams. Details are provided in Supplemental Methods. Confirmation of variants in individuals and in available family members was

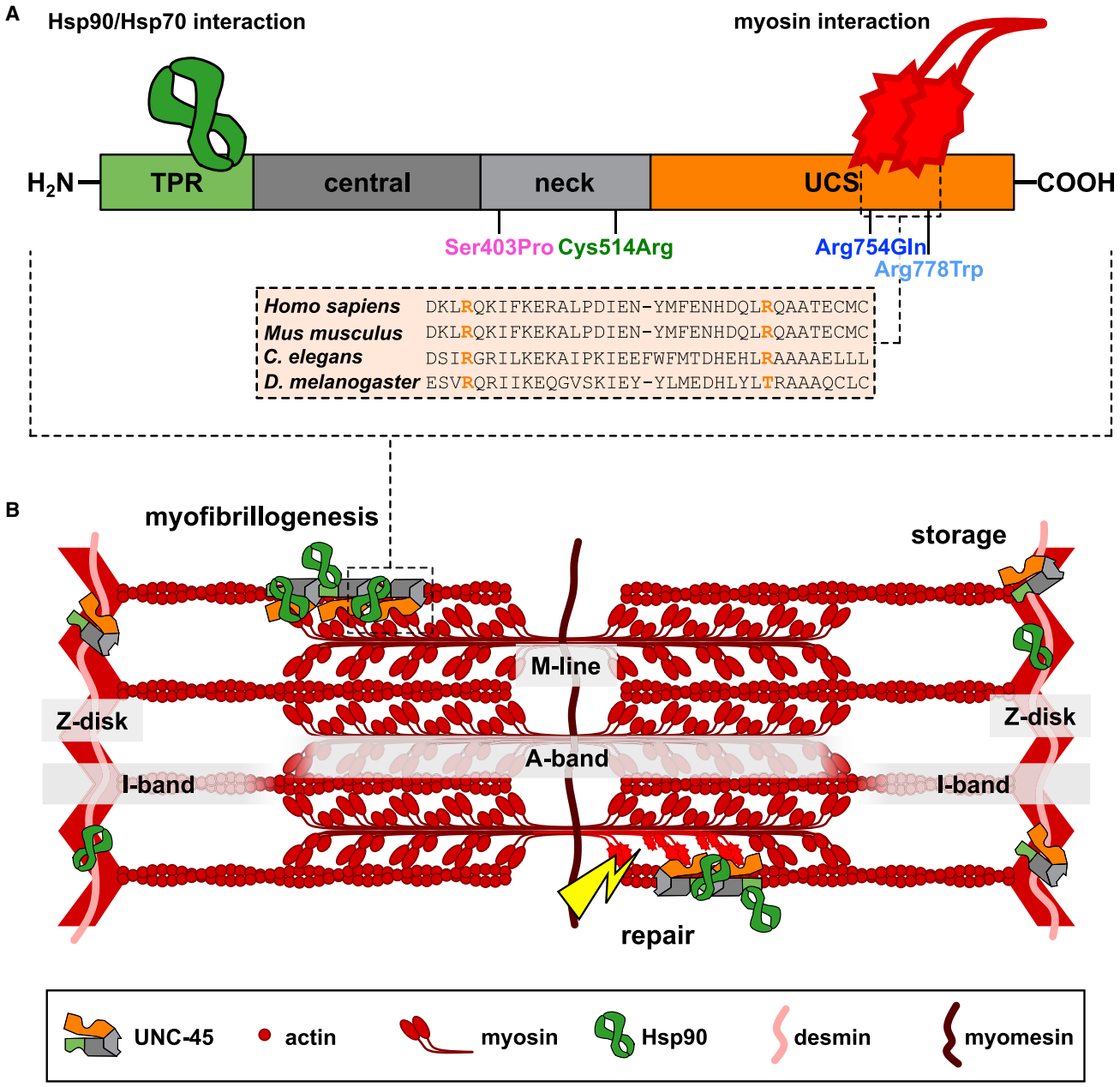

Figure 1. Bi-allelic Variants in the Myosin-Directed Chaperone UNC-45B
(A) UNC-45 contains four domains: an N-terminal TPR domain (light green), a conserved central domain (dark gray), a neck domain (light gray), and a C-terminal UCS domain (orange). The N-terminal TPR domain is important for the interaction with Hsp90 and Hsp70 chaperones, and the C-terminal UCS domain binds directly to the myosin head domain. The recurring *UNC45B* variant p.Arg754Gln (dark blue) and the p.Arg778Trp (light blue) variant impact conserved arginines in the myosin-binding UCS domain. Variants p.Ser403Pro (pink) and p.Cys514Arg (dark green) are located in the UNC-45B neck domain.
(B) Overview of the muscle sarcomere. UNC-45 is involved in myofibrillogenesis, cooperating with Hsp90 to fold and to incorporate myosin into the thick filament. In adulthood, UNC-45 is stored at the Z-disk. Upon injury to the muscle fiber, UNC-45 shuttles to the A-band to help refold damaged myosin.

performed by Sanger sequencing. RNA sequencing on RNA extracted from muscle was pursued for P2, P3, and P4. Details can be found in Supplemental Methods.

Immunoblot

Skeletal muscle biopsy sections from control and affected individuals P1, P2, P9, and P10 were homogenized with lysis buffer containing 4% SDS, 125 mM Tris-HCL (pH 8.8), 40% Glycerol, 500 μM PMSF, and 100 mM DTT. The lysates were sonicated on ice followed by centrifugation (14,000 rpm for 15 min at 4°C). The protein from the supernatants was electrophoresed on NuPAGE 4%–12% Bis-Tris gel (Invitrogen, Carlsbad, CA) under reducing condition followed by a transferring to nitrocellulose membrane (Millipore, Billerica, MA). After block with Odyssey PBS blocking buffer (LI-COR, Lincoln, NE), the membrane was incubated with primary antibody anti-UNC-45B (Sigma-Aldrich, St. Louis, MO) and anti-

desmin (Sigma-Aldrich, St. Louis, MO) overnight at 4°C and subsequently incubated with IRDye 680RD goat anti-rabbit IgG and IRDye 800CW goat anti-mouse IgG secondary antibodies (LI-COR, Lincoln, NE) at room temperature and imaged on the Odyssey CLx Imaging System (LI-COR, Lincoln, NE).

Immunostaining and Microscopy

Pre-cooled 100% methanol fixed 8 μm muscle longitudinal sections were blocked in PBS with 10% goat serum and 0.1% Triton X-100 then incubated with primary antibodies anti-UNC-45B (Sigma-Aldrich, St. Louis, MO) and anti-myomesin (DSHB, Iowa City, IA) overnight at 4°C. The antibody labeling was detected with secondary antibodies Alexa488-conjugated goat anti-mouse IgG and Alexa568-conjugated goat anti-rabbit IgG (Thermo Fisher Scientific, Waltham, MA) for 1 h at room temperature. Prepared muscle sections were imaged with a Zeiss Airy microscope (Zeiss, Germany). Images were analyzed via ImageJ software (National Institutes of Health).

Human UNC-45B Protein Structure Modeling and PyMOL Structural Analysis

For human UNC-45B protein structure modeling, the SWISS-MODEL online tool was used.[21] *C. elegans* UNC-45 (PDB: 4i2z) was indicated as reference crystal structure. For further structural analyses, the PyMOL 2.3.3 software (Schrödinger) and proprietary scripts were used. The modeled human UNC-45B protein structure was displayed and single amino acid mutations inserted with the mutagenesis wizard tool choosing the rotamer with the lowest root-mean-square deviation value. Steric and electrostatic interactions were depicted with the show_bumps plugin and calculations of van der Waals overlaps.

Cloning, Protein Expression, and Purification

Standard molecular biology protocols were used.[22] Human UNC-45B cDNA was cloned into the *E. coli* expression vector pET21a with an N-terminal myc-tag and a C-terminal 6xHIS-tag via the NEBuilder Master Mix (New England Biolabs). We mutated the vector by using the Q5 Site-Directed Mutagenesis Kit (New England Biolabs) to introduce the following variants: p.Arg754Gln, p.Arg778Trp, p.Ser403Pro, and p.Cys514Arg. We mutated a pET21a vector encoding myc-UNC-45-6xHIS amplified from *C. elegans* cDNA by using the Q5 Site-Directed Mutagenesis Kit (New England Biolabs) to introduce the following variants: p.Arg767Gln and p.Arg792Trp. Oligonucleotides used in this study are listed in Table S2. Overexpression in *E. coli* BL21-CP was induced with 100 μM IPTG and carried out at 16°C–18°C for 18–20 h. Subsequently, cells were harvested by centrifugation and lysed by sonication in 50 mM NaH_2PO_4 (pH 8.0), 300 mM NaCl, and 10 mM imidazole. According to the manufacturer's instructions, the tagged proteins were affinity purified by submitting the cleared bacterial lysates to Ni-NTA agarose-binding (QIAGEN). After exchanging the buffer to 20 mM Tris (pH 8.0) and 150 mM NaCl, protein amount was determined by Coomassie staining of SDS-PAGE gels with bovine serum albumin as standard.

Partial Trypsin Proteolysis

For limited proteolysis assays, 2.4 μg purified proteins myc-UNC-45B(WT)-6xHIS, myc-UNC-45B(p.Arg754Gln)-6xHIS, myc-UNC-45B(p.Arg778Trp)-6xHIS, myc-UNC-45B(p.Ser403Pro)-6xHIS, myc-UNC-45B(p.Cys514Arg)-6xHIS, myc-UNC-45-6xHIS, myc-UNC-45(p.Arg767Gln)-6xHIS, and myc-UNC-45(p.Arg792Trp)-6xHIS diluted in PBS (pH 7.4) were incubated with 20 ng of trypsin (SERVA) for 1, 2, 5, 10, 20, 40, or 60 min at room temperature (~22°C) or 37°C. A control reaction was incubated with PBS instead of trypsin for 60 min (time point 0). Reactions were stopped by adding 5× SDS sample buffer (0.25 M Tris-HCl, 10% SDS, 50% glycerol, 0.5 M DTT, and 0.25% bromophenol blue) and flash freezing in liquid nitrogen. After collecting, all samples were boiled at 95°C for 5 min, run on SDS-PAGE gels, and stained with Instant Blue Coomassie stain (Expedeon). Images were taken with an Odyssey CLx Imager (LI-COR Biotechnology) via the 700 nm channel, intact protein bands were quantified with Image Studio Version 5.2 software, and relative fluorescence signal compared to time point 0 was plotted.

Thermal Shift Assay with SYPRO Orange

10 μg purified proteins myc-UNC-45B(WT)-6xHIS, myc-UNC-45B(p.Arg754Gln)-6xHIS, myc-UNC-45B(p.Arg778Trp)-6xHIS, myc-UNC-45B(p.Ser403Pro)-6xHIS, and myc-UNC-45B(p.Cys514Arg)-6xHIS were diluted in ice-cold 20 mM Tris (pH 8.0), 150 mM NaCl, and 2.5× SYPRO Orange protein stain and heated in 0.5°C increments from 10°C to 95°C in a CFX Real-Time PCR Cycler (Bio-Rad). Melt curves were recorded with the FRET channel, normalized to buffer-only control, and fitted to Boltzmann sigmoidal curve regression in GraphPad Prism 5 software. Half maximal temperatures were read as melting temperatures.

Filter Trap Assay and Slot Blot

20 μg purified proteins myc-UNC-45B(WT)-6xHIS, myc-UNC-45B(p.Arg754Gln)-6xHIS, myc-UNC-45B(p.Arg778Trp)-6xHIS, myc-UNC-45B(p.Ser403Pro)-6xHIS, and myc-UNC-45B(p.Cys514Arg)-6xHIS were diluted in ice-cold 20 mM Tris (pH 8.0) and 150 mM NaCl and incubated rotating at room temperature (22°C) for 1 h. Three decreasing amounts of protein solution were loaded onto a 0.2 μm cellulose acetate membrane assembled in a slot blot apparatus (Bio-Rad). The membrane was washed with PBS and 0.2% SDS and retained aggregated protein was assessed by immunoblotting for myc-tag (9E10, Roche).

C. elegans Maintenance and Transgenic Lines

Unless stated otherwise, nematodes were grown at 15°C on nematode growth medium (NGM) plates seeded with the bacterial *E. coli* strain OP50 as a food source according to standard protocols and methods.[23,24] The N2 Bristol strain served as the wild type (WT). Additional strains used in this study are *unc-119(ed4)*III, *unc-45(m94)*III, and *unc-45(m94)*III*; hhIs84[unc-119(+); unc-54::unc-45^{FLAG}]*.[17] For the generation of transgenic rescue strains, plasmids encoding C-terminally FLAG-tagged UNC-45 under the muscle-specific promoter *unc-54*, containing the *unc-119(+)* selection marker, generated by Gazda et al.,[17] were mutated with the Q5 Site-Directed Mutagenesis Kit (New England Biolabs). The following conserved variants were introduced: p.Arg767Gln, p.Arg792Trp, p.Ile422Pro, and p.Cys523Arg. Oligonucleotides used in this study are listed in Table S2. These constructs were bombarded into *unc-119(ed4)* worms as described previously.[25] Microparticle bombardment was done with the Bio-Rad Biolistic PDS-1000/HE with 0.25 in gap distance, 9 mm macrocarrier to screen distance, 28 in of Hg vacuum, and a 1,350 psi rupture disc. Per bombardment, about 1 mg of 1 μm microcarrier gold beads were coated with 8–10 μg linearized DNA. Animals were allowed to recover for 1 h at room temperature and were then transferred to 90 mm NGM plates seeded with *E. coli* OP50 bacteria.

After 3 weeks at 25°C, motile non-*unc* worms were singled and screened for homozygosity. All strains that were used in this study are listed in Table S3.

Motility Assay

For body bend assays, individual young adult worms grown at 25°C were placed in 1 mL M9 buffer (room temperature 22°C) and body bends were counted during 30 s and doubled to calculate body bend counts per minute.

Quantification of I-Bands Assembly

Sarcomere assembly was monitored by labeling F-actin with phalloidin-rhodamine (Invitrogen). Briefly, synchronized young adult worms were fixed in 4% (w/v) paraformaldehyde solution for 20 min at room temperature. After permeabilization of the cuticle in a 3% β-mercaptoethanol solution containing 1% Triton X-100, the F-actin in body wall muscle sarcomeres was stained with phalloidin-rhodamine (Invitrogen). Stained worms were mounted on glass slides and imaged via an Axio Imager.Z1 microscope (Zeiss). The number of I-bands per body wall muscle cell was counted in the same area (between the pharynx and vulva).

Co-immunoprecipitation Studies

For co-immunoprecipitations, synchronized young adult WT worms, *unc-45(m94)*, or worms expressing transgenic, FLAG-tagged UNC-45 were sonicated in lysis buffer (50 mM Tris [pH 8.0], 150 mM NaCl, 1% Triton X-100, and protease inhibitor mix [Roche]), and immunoprecipitation was performed with the μMACS DYKDDDDK Isolation Kit (Miltenyi Biotec) following the manufacturer's instructions. Briefly, 150 μg of worm lysates were incubated with 50 μL Anti-DYKDDDDK MicroBeads for 45 min at 4°C. Immunoprecipitants were washed four times with 200 μL Wash Buffer 1 (150 mM NaCl, 1% Igepal CA-630 [formerly NP-40], 0.5% sodium deoxycholate, 0.1% SDS, and 50 mM Tris HCl [pH 8.0]) on μColumns placed in the magnetic field of a μMACS Separator. Subsequently, immunoprecipitants were washed once in 100 μL Wash Buffer 2 (20 mM Tris HCl [pH 7.5]) and eluted with hot 2× SDS-PAGE sample buffer. Immunoblotting was performed with antibodies against UNC-45, DAF-21 (gift from Richard Morimoto), UNC-54 (mAb5-8-1, DSHB), and Tubulin (T6074, Sigma). Proteins were detected by immunoblotting on PVDF membranes via Amersham ECL Prime (GE Healthcare) in a Bio-Rad ChemiDoc Imager.

Statistical Analysis

For statistical analyses, the GraphPad Prism 5 software was used. Non-parametric statistical tests were used according to the software's recommendations and specified in the respective figure legends and descriptive text. Results are usually given as mean and standard error of the mean (SEM).

Results

Bi-allelic Variants in the Myosin Chaperone UNC-45B in Individuals with Muscle Weakness

We report ten affected individuals from eight independent families clinically manifesting with childhood-onset, progressive proximal and axial muscle weakness and various degrees of respiratory insufficiency. The clinical presentations are summarized in Table 1. Of the identified families, there was one family with three affected siblings (P6, P7, and P8). The only other notable family history was for P1; P1 had a brother with a history of nystagmus and vomiting who was suspected to have a mitochondrial disorder of unknown genetic etiology and who passed away at 3 months of age.

To elucidate the possible origin of the muscle disease, we pursued WES, identifying a recurring homozygous c.2261G>A (p.Arg754Gln) missense variant in *UNC45B* (NM_173167.3) in seven affected individuals from five independent families of various ethnic backgrounds (Table S1). This variant is rare with nine reports in heterozygous state, and none in homozygosity, in the Genome Aggregation Database (gnomAD), and it has an allele frequency of 4.732×10^{-5}. On the protein level, this variant impacts a conserved arginine in the UNC-45B C-terminal UCS domain, which is essential for the interaction with myosin (Figure 1A). P2 was found to be compound heterozygous for a maternally inherited c.2261+5G>C splice variant and a paternally inherited c.2332C>T (p.Arg778Trp) missense variant impacting the UCS domain of UNC-45B. This rare missense variant is predicted to be damaging and reported 45 times in heterozygous state, and none in homozygosity, in gnomAD; it has an allele frequency of 1.593×10^{-4}. P9 was found to have the recurring p.Arg754Gln variant in compound heterozygosity with a rare predicted-to-be-damaging c.1207T>C (p.Ser403Pro) variant impacting the UNC-45B neck domain (Figure 1A). Lastly, P10 was found to be homozygous for a predicted-to-be-damaging c.1540T>C (p.Cys514Arg) missense variant impacting the UNC-45B neck domain. This variant is listed as a rare SNP (rs775340790) with nine reported in heterozygous state, and none in homozygosity, in gnomAD; it has an allele frequency of 3.580×10^{-5}.

UNC45B Variants Manifest Clinically as a Childhood-Onset Myopathy

Six individuals presented with first recognition of axial and proximal weakness in early childhood. These affected individuals reported a slow progression of muscle weakness and remained ambulatory into adulthood. Of interest, these individuals were all homozygous for the recurring c.2261G>A (p.Arg754Gln) variant. Three individuals with other *UNC45B* variants were reported to have a congenital onset of symptoms.

Serum creatine kinase (CK) levels were reported within normal reference ranges in all individuals. Respiratory function ranged from significantly decreased to normal with forced vital capacity (FVC) measurements ranging from 45%–99% predicted. Five individuals had abnormalities on electrocardiogram (ECG), while structural cardiac abnormalities were seen in two. Lower extremity

Table 1. Clinical Characteristics and *UNC45B* Variants Identified

Individual	P1	P2	P3	P4	P5	P6	P7	P8	P9	P10
UNC45B variant	homozygous c.2261G>A (p.Arg754Gln)	c.2332C>T (p.Arg778Trp) (p); c.2261+5G>C (m)	homozygous c.2261G>A (p.Arg754Gln)	homozygous c.2261G>A (p.Arg754Gln)	homozygous c.2261G>A (p.Arg754Gln)	homozygous c.2261G>A (p.Arg754Gln)	homozygous c.2261G>A (p.Arg754Gln)	homozygous c.2261G>A (p.Arg754Gln)	c.2261G>A (p.Arg754Gln) (p); c.1207T>C (p.Ser403Pro) (m)	homozygous c.1540T>C (p.Cys514Arg)
Sex/age at last examination (years)	F/18	F/19	M/27	M/31	M/19	M/53	M/55	M/52	F/6	M/10
Ethnicity / consanguinity	Hispanic/no	Hispanic/no	Turkish/yes	Turkish/yes	Turkish/yes	Thai/no	Thai/no	Thai/no	Sicilian/no	Swedish/no
First symptoms (age)	proximal muscle weakness (6 years)	progressive scoliosis, poor weight gain (7 months)	delayed motor milestones; walked at 2 years	delayed motor milestones; walked at 2 years	proximal muscle weakness (4 years)	proximal muscle weakness (6 years)	proximal muscle weakness (5 years)	muscle weakness (6 years)	congenital hypotonia, weak cry, feeding difficulties; delayed motor milestones; walked at 3 years	congenital hypotonia, knee contractures, feeding and respiratory difficulties
Distribution of weakness	slowly progressive axial and proximal weakness	axial and proximal weakness	slowly progressive proximal weakness	slowly progressive proximal weakness	slowly progressive proximal weakness	slowly progressive childhood onset proximal weakness	slowly progressive childhood onset proximal weakness	slowly progressive proximal muscle weakness	proximal weakness	axial weakness
Muscle bulk	calf hypertrophy	calf hypertrophy	–	calf hypertrophy	calf hypertrophy; atrophy of shoulder girdle	–	–	calf hypertrophy	–	moderate generalized atrophy
CK (U/L) [reference range]	130 [26–192]	normal	220 [140–200]	137 [140–200]	56	149 [1–190]	95 [1–190]	241 [1–190]	35 [1–150]	normal
EMG	mildly neurogenic	myopathic	myopathic	myopathic	not myopathic	myopathic	N/A	N/A	N/A	myopathic
Muscle biopsied (age)	vastus lateralis (18 years)	quadriceps (5 years)	deltoid (26 years)	deltoid (31 years)	quadriceps (13 years)	biceps (43 years)	N/A	N/A	vastus lateralis (5 years)	vastus lateralis (10 years)

(*Continued on next page*)

Table 1. ***Continued***

Individual	P1	P2	P3	P4	P5	P6	P7	P8	P9	P10
Histologic findings	moderate variation in fiber size with rounded and elongated atrophic fibers and numerous internalized nuclei; areas devoid of oxidative staining, suggestive of cores; uniform type 1 fiber predominance	slight variation in fiber size with increased number of internalized nuclei; areas devoid of oxidative staining, consistent with eccentric cores; uniform type 1 fiber predominance	large, irregular areas of oxidative defects and myofibrillar disorganization; evidence of fuschinophilic inclusions on trichrome stain; type 1 fiber predominance	large, irregular areas of oxidative defects and myofibrillar disorganization; evidence of fuschinophilic inclusions on trichrome stain; type 1 fiber predominance	severe fatty replacement; increased number of internalized nuclei in the remaining muscle fibers	moderate variation in fiber size with increased number of internalized nuclei; evidence of ring fibers, moth-eaten and core-like fibers on NADH stain; ring- and necklace-like cytoplasmic bodies and rimmed vacuoles on trichrome stain; type 1 fiber predominance	N/A	N/A	variation in fiber size with increased number of internalized nuclei; evidence of fuschinophilic inclusions on trichrome stain; large, irregular areas of oxidative defects and myofibrillar disorganization	type 1 fiber predominance; occasional internalized nuclei; occasional fibers with areas devoid of oxidative staining
Ultrastructural findings (on EM)	large areas of disorganization and some diffusion of the Z-line material	large areas of disorganization and some diffusion of the Z-line material	cytoplasmic bodies and granulo-filamentous aggregates	cytoplasmic bodies and granulo-filamentous aggregates	N/A	non-diagnostic	N/A	N/A	N/A	N/A
FVC (% predicted)	62% (18 years)	45% (19 years)	60% (26 years)	81% (31 years)	80% (19 years)	N/A	N/A	N/A	N/A	99% (13 years)
Cardiac evaluations	echocardiogram, normal; ECG, normal (18 years)	aortic coarctation and IVC s/p surgery	echocardiogram, normal; ECG, normal (26 years)	echocardiogram, normal; ECG, tachycardia (31 years)	echocardiogram, normal; ECG, normal (15 years)	echocardiogram, normal; ECG, incomplete R bundle branch block (53 years)	ECG, left ventricular hypertrophy (55 years)	ECG, complete R bundle branch block, tachycardia (50 years)	ECG, normal (5 years)	aortic coarctation and VSD s/p surgery
Other	dysphagia, fatigue	episode of supraventricular tachycardia, primary amenorrhea	dysphagia	dysphagia	fatigue	–	episode of pneumonia with respiratory failure, difficulty weaning of ventilator; nighttime BiPAP (55 years)	–	ankle contractures and prominent calcaneus	mild ophthalmoplegia, joint hypermobility, premature adrenarche

Abbreviations are as follows: CK, creatine kinase; ECG, electrocardiogram; EM, electron microscopy; EMG, electromyography; F, female; FVC, forced vital capacity; IVC, inferior vena cava; m, maternal; M, male; N/A, not available; NADH, nicotinamide adenine dinucleotide; p, paternal; R, right; s/p, status post; VSD, ventricular septal defect.

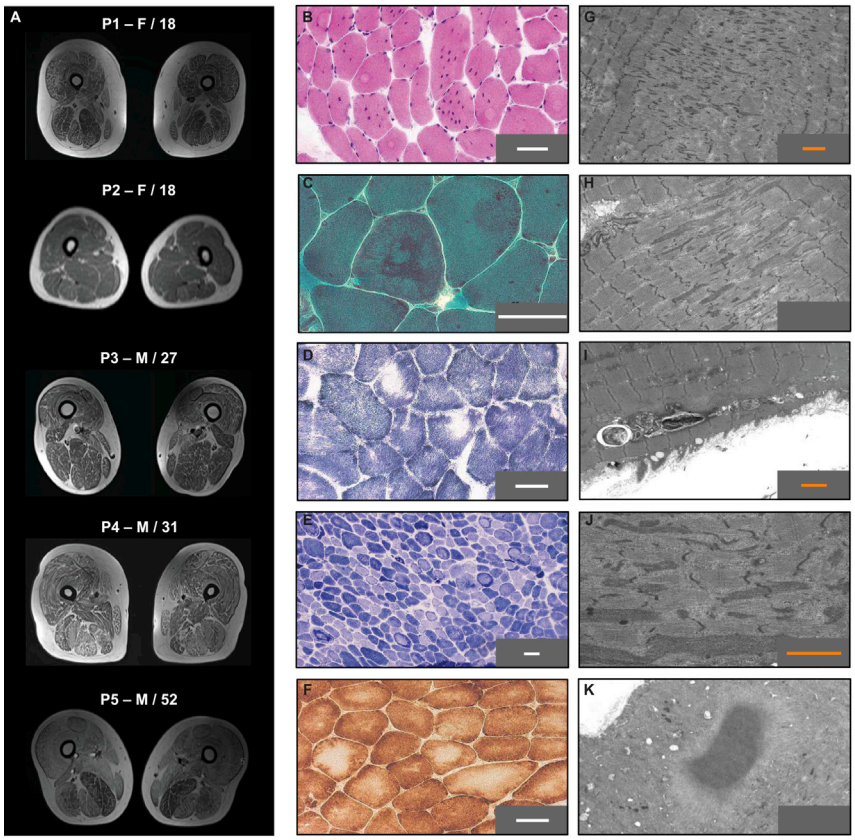

Figure 2. Muscle Magnetic Resonance Imaging and Histological Findings in Individuals with *UNC45B*-Related Myopathy

(A) Lower extremity muscle MR imaging was available for five (P1–P5) individuals and showed mild fat infiltration evident in all lower extremity muscles, resulting in a marbled-like appearance. In individuals P1, P4, and P5, there is abnormal (increased) T1 signal without an apparent pattern of muscle involvement except for relative sparing of the semimembranosus muscle in individuals P1 and P5. P1 and P3 had evidence of mild, generalized muscle atrophy, whereas in P2, P4 and P5, muscle bulk appeared normal.

(B–K) *UNC45B*-related myopathy manifests histologically with unstructured cores. On histological analyses there are findings of the following: increased internalized nuclei with numerous multinucleated fibers seen on H&E staining (P1) (B); uneven deposits of fuchsinophilic material is seen on GT staining (P4) (C); core-like regions often located along the periphery of fibers and consistent with eccentric cores are seen on SDH staining (P3) (D); areas of increased staining along the periphery of fibers with decreased staining centrally is seen on NADH staining (P6) (E); and large irregular areas of decreased staining seen on COX staining (P4) (F); on EM, there are findings of myofibrillar disarray (P3) (G); diffusion of Z-line material (P4) (H); autophagy lesions (P3) (I); wide bands of diffusion of the Z-line material that have spread in the disorganized areas (P3) (J); and a cytoplasmic body (P4) (K); white scale bar represents 50 μm; orange scale bar represents 5 μm.

muscle MR imaging revealed evidence of mild fat infiltration of most muscles, resulting in a marbled-like appearance but without an emerging clear pattern of muscle involvement (Figure 2A).

UNC45B-Related Myopathy Manifests Histologically with Eccentric Cores

Histological analysis of the muscle biopsies was performed in seven individuals (Figures 2B–2K). Hematoxylin and eosin (H&E) stain showed variation in fiber size with internalized nuclei, resulting in multinucleated fibers in five individuals (Figure 2B). On Gömöri Trichrome (GT) stain, a few fibers had evidence of uneven aspects with deposit of fuchsinophilic material in three biopsies (Figure 2C), and there was evidence of apparent cytoplasmic bodies as well as rimmed vacuoles in one. On oxidative staining with succinic dehydrogenase (SDH), nicotinamide adenine dinucleotide (NADH), and cytochrome oxidase (COX), large irregular areas of oxidative defects were identified in numerous muscle fibers. In particular, in five of the seven biopsies reviewed, SDH staining and COX staining revealed more defined areas of reduced oxidative activity with core-like regions often located along the periphery of fibers, consistent with eccentric cores (Figures 2D and 2F). In contrast, in two biopsies, there were areas of reduced NADH staining alternating with areas of increased staining along the periphery of fibers. On ATPase stains, there was evidence of type I fiber predominance and areas of absence/reduction of ATPase activity, particularly in the periphery of fibers, corresponding to the areas resembling eccentric cores on the oxidative stains (Figure 2E). Electron microscopy (EM) was performed in four individuals (Figures 2G–2K). In longitudinal sections, there were large areas of myofibrillar disorganization that extended the entire width of the fiber that appeared devoid of mitochondria, thus resembling unstructured cores. In transverse sections, well-demarcated unstructured cores were seen in subsarcolemmal regions. In addition, wide dark bands of diffused Z-line-derived material were observed and are reminiscent of myofibrillar material. More rarely, cytoplasmic bodies (Figure 2K) and rod-like inclusions were seen, and autophagy material was observed in some fibers.

Fiber Contractile Function Is Normal in P1 UNC-45B Muscle

Muscle contraction is affected by the cyclic interaction between the myosin cross-bridges and actin as an adenosine triphosphate (ATP) hydrolysis-dependent process.[26] The maximum force that a muscle fiber can generate is dependent on the rate of myosin cross-bridge cycling kinetics. To evaluate whether force generation in UNC-45B muscle was impaired in this assay, we compared the

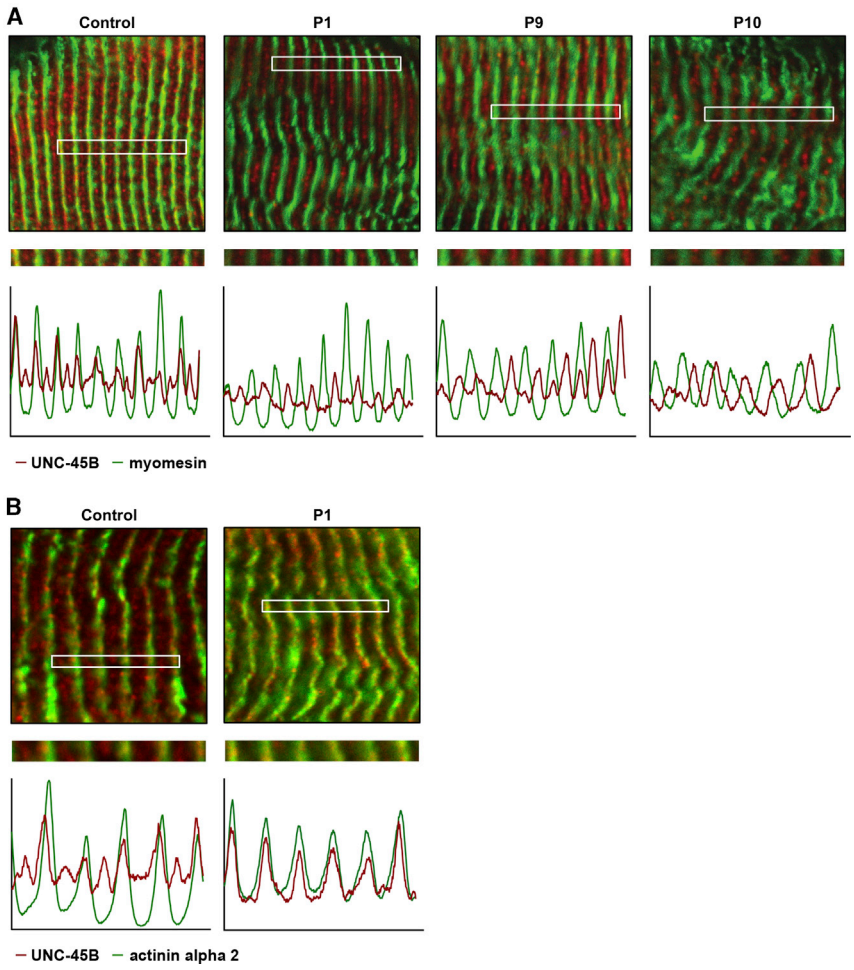

Figure 3. Mislocalized UNC-45B Protein in Affected Individuals' Muscle

(A) Longitudinal sections of muscle biopsies of control and P1, P9, and P10 stained for UNC-45B (red) and M-line protein myomesin (green) (top row). UNC-45B is reduced in the M-line and mislocalized from the A-band, around the M-line, to the Z-line in these three individuals compared to control. Overlay of intensity profile of UNC-45B and myomesin (bottom row) from the cropped area (middle row) shows mislocalization of UNC-45B away from the A-band to the Z-disk.

(B) Longitudinal sections of muscle biopsies of control and P1 stained for UNC-45B (red) and Z-disk protein α-actinin (green), revealing colocalization of UNC-45B at the Z-line. Overlay of intensity profile of UNC-45B and α-actinin in P1 from the cropped area (middle row) shows loss of co-location of UNC-45B with the M-line.

mechanics of permeabilized single muscle fibers from P1 (homozygous c.2261G>A) to controls. Rate of tension redevelopment (K_{tr}) was used as a parameter reflecting the rate of both cross-bridge attachment and reattachment, while tension cost reflects the rate of myosin cross-bridge detachment from actin determined by measuring the ATP utilization during force generation. P1 muscle expressed predominately myosin heavy chain (MHC) type I fibers. Contractile properties depend on MHC composition, and therefore, we compared contractile data to controls in whom MHC type I and type II fibers were separated. Our data showed normal fiber contractile performance with no difference in maximal tension generated by UNC-45B fibers compared to controls (Figure S1A). The calcium sensitivity of force, the Ca^{2+} concentration needed for 50% of maximal force generation, was also normal in P1 muscle compared to control (Figure S1B). Overall, single fiber mechanics in P1 muscle tissue showed normal cross-bridge cycling kinetics with expected tension costs compared to control (Figures S1C and S1D).

UNC-45B Is Mislocalized in Affected Individuals' Muscle

Immunofluorescence localization studies were performed with myomesin, a major structural protein of the M-line, and α-actinin, a Z-line protein, as markers.[27] Whereas, in control muscle, UNC-45B localized to the A-band around the M-line as expected, in affected individuals, there appears to be a loss of the residual UNC-45B at the M-line, suggestive of mislocalization away from the A-band to the Z-disk (Figures 3A and 3B). The specificity of the UNC-45B antibody was confirmed in control muscle (Figure S2).

The Recurring *UNC45B* c.2261G>A Variant Acts as a Complex Hypomorph Splice Variant

UNC45B appears to be intolerant to complete bi-allelic loss of function, which is in accordance with the essential role of UNC-45 in *C. elegans*.[28–30] Therefore, we did not observe individuals with bi-allelic null variants, and no homozygous null variants are listed in gnomAD.[31] Haploinsufficiency of *UNC45B*, however, does not appear to cause a severe or early myopathy because individuals heterozygous for a loss-of-function *UNC45B* variant are reported in gnomAD. The recurring c.2261G>A *UNC45B* variant affects the last base pair (G) of exon 17 and is adjacent to the splice donor site, thus potentially interfering with normal splicing (Figure 4A).[32,33] To investigate this possibility, we analyzed muscle RNA sequencing, available for two individuals (P3 and P4, both homozygous for the c.2261G>A *UNC45B* variant) (Figure S3A). This transcript analysis revealed a five-fold reduction of *UNC45B* transcripts compared to controls and furthermore indicated that two detectable *UNC45B* splice products were generated from the mutant allele (Figure S3B). The first detectable transcript encodes the full-length protein containing the

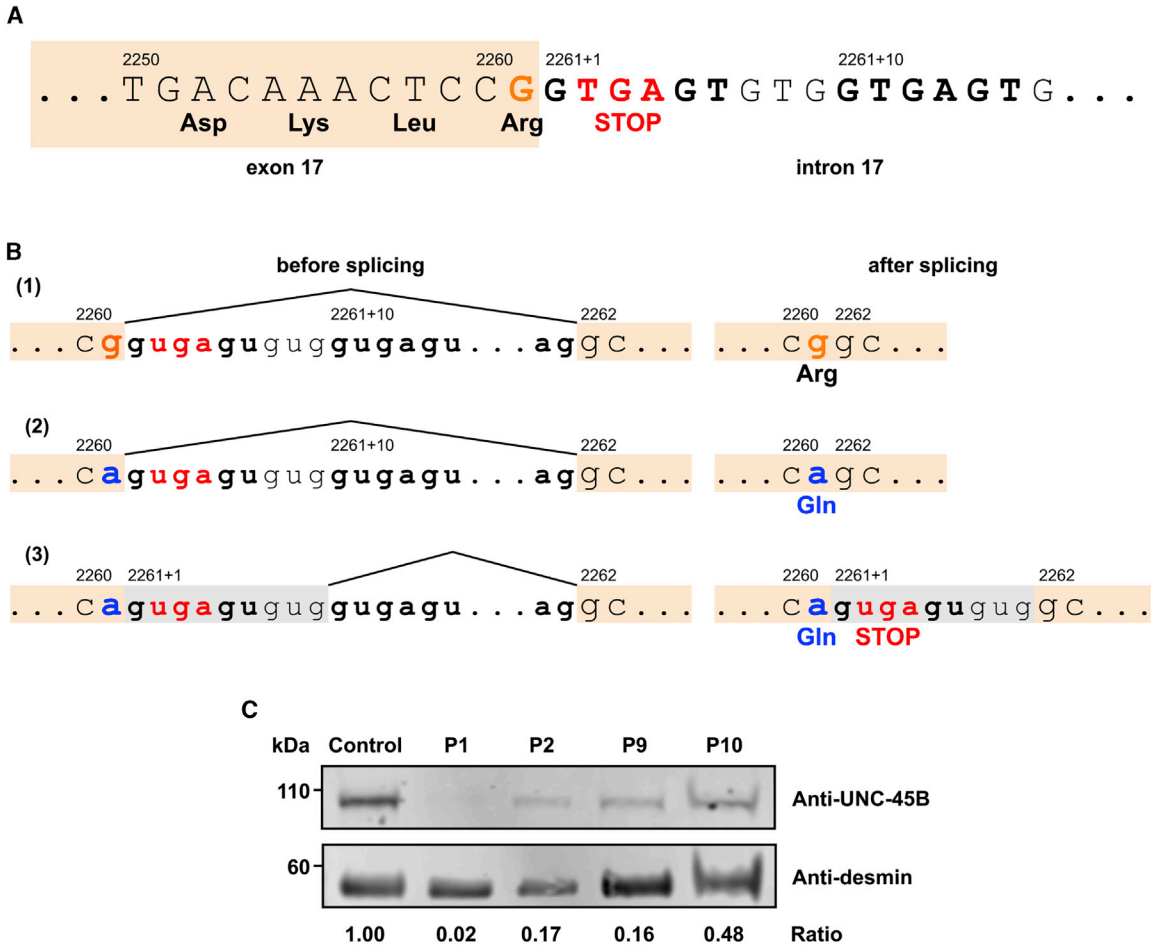

Figure 4. *UNC45B* Variant c.2261G>A Creates a Complex Hypomorph Splice Variant

(A) The last base pair of exon 17 in *UNC45B* c.2261G (orange) is adjacent to the splice donor site of intron 17 (bold black). The c.2261G>A transition, located in the exonic part of the 5′ recognition sequence (G-G-U-G-A-G-U), leads to the activation of a nearby cryptic splice donor site (bold black). The resulting spliced mRNA transcript is elongated by 9 additional bases including an in-frame STOP codon (bold red).

(B) Schematics of (1) normal *UNC45B* exon 17–18 splicing and of the two splice products seen in *UNC45B* c.2261G>A muscle: (2) full length product including the p.Arg754Gln substitution and (3) activation of the nearby cryptic splice donor site generating an elongated splice product that includes an in-frame STOP codon.

(C) Immunoblot analysis of UNC-45B in muscle extracts from P1, P2, P9, and P10 compared to control. Quantification shows a significant reduction of UNC-45B in P1, P2, P9, while levels in P10 were slightly reduced. Mouse monoclonal anti-desmin was used as a loading control.

p.Arg754Gln missense variant. The second transcript results from altered splicing due to interruption of the normal splice donor and subsequent activation of a nearby intronic cryptic splice donor site, c.2261+10 (Figure 4B). The resulting splice product extends exon 17 into the intron, causing the inclusion of an in-frame STOP codon. This nonsense transcript is unstable and most likely subject to nonsense-mediated decay. A low level of the elongated nonsense transcript escaped mRNA decay and was therefore detectable on muscle RNA sequencing. From this we conclude that the c.2261G>A *UNC45B* variant results in a hypomorphic splice variant. The effect is a situation in which the majority of transcripts are mis-spliced to include a premature termination codon with predominant degradation before translation occurs, while any residual correctly spliced full-length transcript will result in a protein containing the p.Arg754Gln missense variant.

RNA sequencing and reverse transcription of mRNA with subsequent cDNA sequencing in P2 muscle extracts revealed allelic imbalance toward the p.Arg778Trp variant, while the c.2261+5G>C splice variant resulted in activation of the same nearby intronic cryptic donor site as seen for the c.2261G>A variant and is thus expected to lead to the same nonsense-mediated decay (Figures S3C–S3H). In summary, the c.2261G>A and the c.2261+5G>C *UNC45B* variants both impact the proper splicing of the mRNA and, thus, the stability of the *UNC45B* mRNA.

To investigate the impact of the *UNC45B* variants on the protein level, we performed immunoblot on muscle

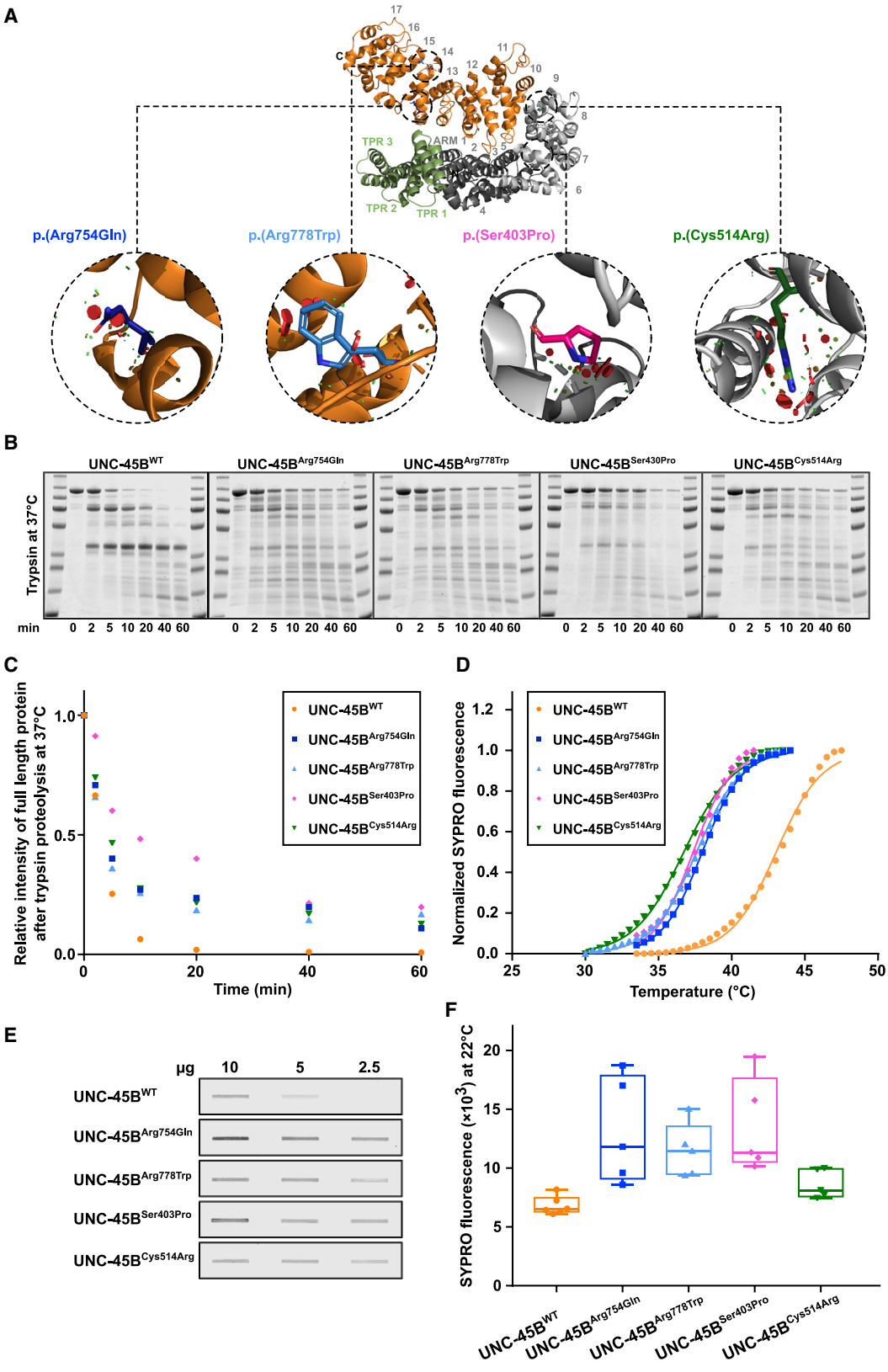

Figure 5. UNC-45B Mutant Proteins Are Prone to Aggregation

(A) Structure of human UNC-45B based on the *C. elegans* UNC-45 3D structure (PDB: 4i2z)[17] modelled with Swiss-Model,[21] and corresponding residues mutated in PyMOL to display the reported variants. The recurring p.Arg754Gln (dark blue) and the p.Arg778Trp (P2) *UNC45B* variant (light blue) impact conserved arginine residues in the myosin-binding UCS domain (orange) and can be precisely mapped to helices 1 and 3, respectively, in the armadillo (ARM) repeat 14. ARM 14 is located in the hinge region, which connects the C-terminal half of the UCS domain (ARM repeats 14–17) with the N-terminal half (ARM repeats 10–13) and forms part of the myosin-binding

(legend continued on next page)

extracts from P1, P2, P9, and P10. All four individuals showed a significant reduction of UNC-45B compared to controls (Figure 4C).

Missense Variants Impact Conserved UNC-45B Domains

The UNC-45B amino acid sequence is highly conserved down to invertebrates, which allowed us to explore the structural impacts of variants on the basis of the recently elucidated structure of *C. elegans* UNC-45.[14,16,17] Both arginine residues altered in our cohort (Arg754 and Arg778) are part of helices 1 and 3, respectively, in the armadillo (ARM) repeat 14 (Figure 5A). ARM 14 is located in the hinge region, which connects the C-terminal half of the UCS domain (ARM repeats 14–17) with the N-terminal half (ARM repeats 10–13), forming part of the myosin-binding canyon. Exchanging Arg754 for glutamine does not seem to drastically interfere with the surrounding structures, according to PyMOL calculations of van der Waals overlaps. Conversely, exchanging the positively charged Arg778 for a bulky hydrophobic tryptophan would most probably sterically interfere with its surroundings, up to the possible shifting of the overall structure of the UCS domain. P9 was found to carry the recurring p.Arg754Gln missense in compound heterozygosity with a p.Ser403Pro missense located in the UNC-45 neck domain. Ser403 is conserved in zebrafish UNC-45B, but position 403 appears to have a broader tolerance for other amino acids, featuring a threonine in *Drosophila* and isoleucine in *C. elegans* UNC-45. Its functional importance, therefore, may be restricted to vertebrates but needs to be investigated further.

Close cooperation of the chaperones Hsp90 and Hsp70 with UNC-45 allows for the precise temporal and spatial control of incorporating myosin into contractile muscle thick filaments.[1,17,34] P10 was found to be homozygous for a p.Cys514Arg missense variant, which impacts the neck domain, and is therefore the only individual in this series without an UNC-45 UCS domain allele. Given that the UNC-45 neck domain confers flexibility and allows the exact positioning of the UCS and the TPR domains to one another, structural interference in this region is likely to impact protein function. The affected cysteine residue is buried in the inner structure of ARM 9 in the neck domain of UNC-45. Exchanging a cysteine for a positively charged arginine would most probably lead to steric hindrance and electrostatic interference within the protein structure (Figure 5A).

Recombinant UNC-45B Variants Are Prone to Aggregation

To further elucidate the structural impacts of the *UNC45B* variants, we recombinantly expressed the UNC-45B mutant proteins in *E. coli* and subjected them to time-dependent partial trypsin proteolysis experiments at room temperature (22°C). All mutant variants seemed less susceptible to proteolysis than the WT; the p.Ser403Pro variant showed the most pronounced difference (Figures S4A and S4B). Repeating the partial trypsin proteolysis assay at the physiological temperature 37°C corroborated that trypsin proteolysis was delayed in the mutant variants, and the p.Ser403Pro variant was significantly different in the non-parametric Friedman test (Figures 5B and 5C, Table S4). In addition, we performed thermal shift assays (TSAs) with the protein stain SYPRO Orange to determine the melting temperatures of the recombinant proteins in solution. The stain intercalates with gradually exposed hydrophobic residues on the protein's surface, allowing for melting temperature estimation based on the half-maximal SYPRO fluorescence in a Boltzmann approximation. The assay revealed that all variant proteins have a lower melting temperature (p.Arg754Gln, 38.18 ± 0.05145°C; p.Arg778Trp, 37.85 ± 0.04907°C; p.Ser403Pro, 37.88 ± 0.1241°C; and p.Cys514Arg, 36.90 ± 0.03901°C) compared to WT (43.16 ± 0.04358°C) in the Tris-based buffer (Figure 5D, Tables S5 and S6). Exposed hydrophobic residues at a lower temperature might suggest aggregation tendency. On these grounds, we subjected the recombinant mutant variants to a filter trap assay to search for aggregates after incubation at room temperature (22°C). A subsequent slot blot confirmed the suspected higher aggregation of the

canyon. The p.Ser403Pro (pink, P9) and p.Cys514Arg (dark green, P10) variants impact the UNC-45B neck domain. Van der Waals overlaps of the newly incorporated amino acid residues with the unmodified protein structure are depicted as red disks.
(B) Purified UNC-45B^{WT}, UNC-45B$^{p.Arg754Gln}$, UNC-45B$^{p.Arg778Trp}$, UNC-45B$^{p.Ser403Pro}$, and UNC-45B$^{p.Cys514Arg}$ buffered solutions were subjected to partial proteolysis with trypsin at 37°C, and samples were loaded on SDS-PAGE gels for separation. Coomassie-stained gels of one of two repetitions are shown.
(C) Quantification of full-length protein (~109 kDa) compared to time point 0 at 37°C of two repetitions. Mean and SD can be found in Table S4.
(D) Purified UNC-45B^{WT}, UNC-45B$^{p.Arg754Gln}$, UNC-45B$^{p.Arg778Trp}$, UNC-45B$^{p.Ser403Pro}$, and UNC-45B $^{p.Cys514Arg}$ buffered solutions were slowly heated from 10°C to 95°C in the presence of SYPRO Orange protein stain. Boltzmann sigmoidal curves were fit to normalized combined melt curves of three experiments. Half maximal temperatures indicate melting temperatures in the Tris-based buffer. Mean and SD can be found in Table S5.
(E) Slot blot of purified UNC-45B^{WT}, UNC-45B$^{p.Arg754Gln}$, UNC-45B$^{p.Arg778Trp}$, UNC-45B$^{p.Ser403Pro}$, and UNC-45B$^{p.Cys514Arg}$ Tris-buffered solutions incubated for 1 h at room temperature filtered through a 0.2 μm acetyl-cellulose membrane. Three decreasing amounts of protein solution were blotted for comparison.
(F) Baseline-subtracted SYPRO fluorescence values at 22°C obtained in two experiments in (D) are plotted for each protein solution. No significant differences between WT and mutant proteins were found in non-parametric Kruskal-Wallis test.

mutant variants compared to the WT to a similar degree as the absolute SYPRO fluorescence at 22°C indicated (Figures 5E and 5F). Further increased aggregation propensity of the mutant variants around the melting temperature of 37°C could also explain the observed delay in *in vitro* proteolysis because a fraction of the substrate was sequestered in trypsin-inaccessible aggregates. Together, biochemical analyses of the recombinant UNC-45B mutant variants suggest that amino acid substitutions at the here-reported positions will most likely lead to structural changes in UNC-45B.

Myopathy-Related UNC-45B Mutant Missense Proteins Cannot Rescue a Conditional Loss-of-Function Allele

To test for the functional performance of the disease-associated UNC-45B UCS variant proteins in myosin assembly, we used an *in vivo* rescue approach in *C. elegans* described previously.[17] Temperature-sensitive (*ts*) *unc-45(m94)* mutant worms exhibit a severe movement defect and disarrangement of the otherwise highly conserved sarcomere organization when grown at the non-permissive temperature of 25°C.[34] By expressing the corresponding *C. elegans* UNC-45 variants in conditional loss-of-function worms, we analyzed to what degree muscle function of the *unc-45 ts* mutant could be restored. When transferred to a liquid medium, worms swim by thrashing their bodies sideways. This agile movement is almost completely abolished in the *m94*-allele-containing mutant worms grown at 25°C. Integrated transgenes expressing the ortholog protein of the p.Arg778Trp variant, UNC-45(p.Arg792Trp); the p.Ser403Pro variant, UNC-45 (p.Ile422Pro); and the p.Cys514Arg variant, UNC-45(p.Cys532Arg), were unable to rescue the movement phenotype of the *unc-45(m94)* strain. Body bend/thrashing counts of young adult worms in liquid medium were only slightly improved compared to WT levels for the UNC-45 (p.Arg792Trp) and UNC-45 (p.Ile422Pro) transgenes. In contrast, worms expressing the UNC-45 (p.Cys532Arg) transgene were as impaired as *unc-45(m94)* without transgenic expression (Figure 6A). Assessing population motility of 60 worms via an ARENA WMicrotracker (NemaMetrix) reproduced the motility defect on a solid agar surface (Figure 6C). These data suggest that the c.2332C>T (p.Arg778Trp), the c.1207T>C (p.Ser403Pro), and the c.1540T>C (p.Cys514Arg) variants very likely affect UNC-45B protein function. In contrast, expression of the ortholog protein of the p.Arg754Gln variant, UNC-45 (p.Arg767Gln), in the *unc-45(m94)* background was able to rescue the defect in movement (Figures 6A and 6C). Although not possessing polynuclear myofibers, sarcomere organization and components in *C. elegans* body wall muscle cells are highly conserved: thick filaments are formed by myosin heavy chains A and B and actin fibers from thin filaments, and Z-disk-equivalent dense bodies are formed by α-actinin and integrins.[35] Sarcomere numbers in body wall muscle cells can be assessed by established staining methods, which allow counting periodically organized sarcomeric components. In accordance with motility assays and contrary to the UNC-45 (p.Arg767Gln) transgenic rescue, the UNC-45 (p.Arg792Trp), the UNC-45 (p.Ile422Pro), and the UNC-45 (p.Cys532Arg) transgenic rescues showed no improvement of the sarcomeres of the *m94 ts* allele in phalloidin-staining of filamentous F-actin-containing I-bands (Figures 6D and 6E).

On the basis of the known mechanistic role of the UCS domain,[16,17,34] the corresponding arginine residues in *C. elegans* can be precisely linked to myosin binding. Whereas FLAG-tagged UNC-45(p.Arg767Gln) was able to bind to the substrate myosin heavy chain B (MHC B/UNC-54) in co-immunoprecipitation experiments (Figure 6F), UNC-45 (p.Arg792Trp) was not able to pull down MHC B from worm lysates, suggesting conformational changes of the myosin-binding canyon in the UCS domain for the variant protein. Conceivably, binding to *C. elegans* Hsp90 ortholog DAF-21 via the TPR domain was not impaired in both variant proteins.

However, it is noteworthy that in these transgenic rescue experiments we cannot control for the additional hypomorphic deficiency situation of the p.Arg754Gln/p.Arg767Gln variant. Although the p.Arg767Gln-encoding transgene is expressed at a slightly lower level than the WT transgene in these experiments (Figure 6B), it is still able to rescue the muscle phenotype and bind to MHC B. Reduced levels of UNC-45 are detrimental for muscle development.[29,36] Our results therefore suggest, that the *UNC45B* p.Arg754Gln missense is not the primary cause of pathogenicity in those individuals, and the disease is most likely driven by the reduction in total UNC-45B due to degradation of the majority of mis-spliced transcripts.

Discussion

We report ten individuals from eight independent families with a largely consistent clinical phenotype of early-onset, slowly progressive muscle weakness manifesting with axial and proximal weakness and respiratory involvement with muscle histotype findings including eccentric and unstructured cores as well as ultrastructural findings suggestive of an accumulation of myofibrillar material. All individuals were found to have bi-allelic variants in *UNC45B,* which encodes a highly conserved myosin-specific chaperone involved in assembly, function, and maintenance of type II myosin, facilitating assembly and function of striated muscle contraction. UNC-45, together with the general chaperones Hsp70 and Hsp90, forms a transient anchoring chain that organizes a properly spaced assembly line, locking the myosin head into actin-bound confirmation by facilitating hydrolysis.[17] This repeating unit stabilizes the thick filament and inhibits the myosin power stroke.[37] A single individual with myopathy who was homozygous for the c.2261G>A variant was previously reported, suggesting a tentative disease association; however, the precise

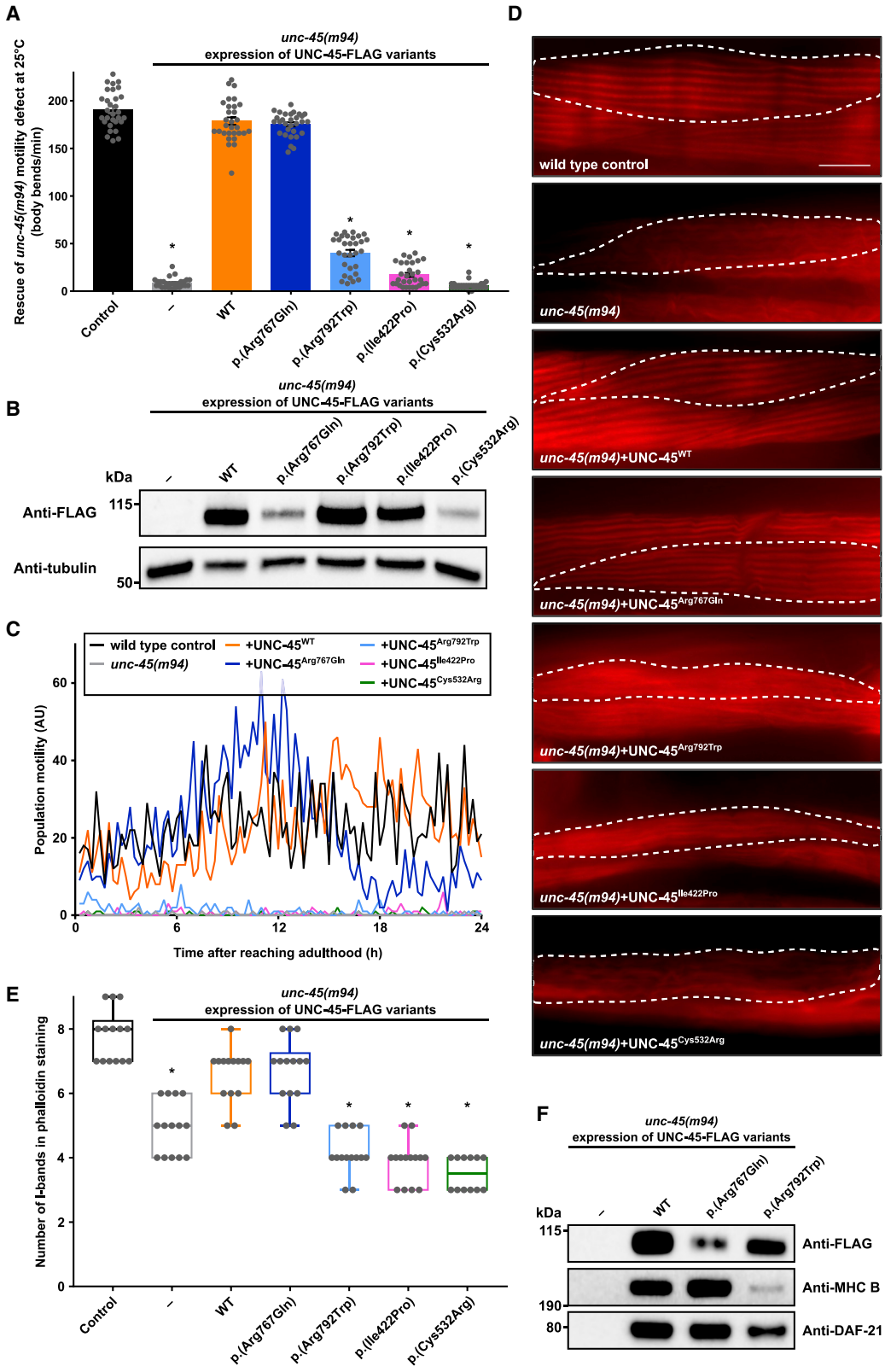

Figure 6. Various Missense UNC-45 Mutant Proteins Cannot Rescue a Conditional Loss-of-Function Allele

Transgenic UNC-45$^{p.Arg792Trp}$, UNC-45$^{p.Ser422Pro}$, and UNC-45$^{p.Cys532Arg}$ mutant proteins are unable to rescue the motility defect of *unc-45(m94)* worms grown at the restrictive temperature of 25°C, whereas UNC-45$^{p.Arg767Gln}$ rescues the *m94* motility defect.

(A) Body bends of 30 young adult *unc-45(m94)* worms expressing the indicated UNC-45 variants were counted in at least three different experiments. Values are mean ± SEM; *p < 0.0001 compared to control in non-parametric Kruskal-Wallis test.

(B) Expression of UNC-45-FLAG transgenes in young adult *unc-45(m94)* worms.

(legend continued on next page)

interaction of UNC-45B with myosin in muscle function and disease remained poorly understood.[38]

Early-onset myopathies are a clinical and genetic heterogeneous group of disorders of variable severity in which approximately half of the individuals do not have a confirmed genetic etiology.[39,40] Significant extraocular and facial weakness was notably absent in the *UNC45B*-affected individuals reported here, which is in contrast to the core myopathies due to pathogenic variants in *RYR1* (MIM: 180901), *CACNA1S* (MIM: 114208), or *SPEG* (MIM: 615950) in which involvement of the extraocular and facial muscles is typically seen.[41–43] Of the ten individuals reported here, tachycardia was noted in two, while two individuals presented with structural cardiac changes (VSD and aortic coarctation). UNC-45B is highly expressed in human cardiac tissue and has an important evolutionary role in cardiac contractility.[28,44,45] Thus, the lack of more significant functional cardiac involvement in our cohort is noteworthy; however, it remains unclear whether a more severe cardiac phenotype might evolve.

Pathogenic variants in various myosin chains, including *MYH2* (MIM: 160740) and *MYH7* (MIM: 160760), are a known cause of myopathies of variable severities, and they have clinical and histological findings similar to our *UNC45B*-affected individuals.[46,47] Various genetically defined core myopathies with clinical overlap, including *RYR1*- and *MYH7*-related myopathies, can present with a characteristic and recognizable pattern of muscle involvement and sparing when assessed by muscle imaging.[48–50] However, a selective and potentially diagnostic pattern of muscle involvement was thus far not evident on muscle imaging in our *UNC45B* cohort. Instead, imaging revealed a fairly uniform involvement of all muscles and a possible hint of relative sparing of the semimembranosus muscle of the hamstring group. In contrast to a dystrophic process, which is characterized by uniform fatty infiltration, or to a neurogenic process in which we typically see a coarse "moth-eaten" appearance on MR imaging, the muscle of *UNC45B*-affected individuals had a characteristic "marbled-like" appearance on fat-sensitive T1 MR imaging sequences, which could potentially be a characteristic and thus diagnostically helpful finding.[49] Given the potential developmental role of UNC-45B,[14,15] it is of note that the myofibrillar apparatus in the individuals reported here appears to be normal at baseline with normal *in vitro* contractile performance and myosin cross-bridge cycling. Therefore, we hypothesize that with ongoing use and stress on the muscle fibers over time, the sarcomere is inadequately maintained because of reduction in myosin chaperone availability and/or functioning. Repair capacity may be overloaded, and sarcomeres start disintegrating, thereby giving rise to the unstructured cores and the accumulation of Z-line/myofibrillar material consistently seen in the UNC-45B muscle biopsies.

Consistent with an abnormal function of UNC-45B in relation to the sarcomere, muscle immunofluorescence findings in three biopsies reveal abnormal localization of the residual UNC-45B away from the M-line-centered A-band where the myosin heads are located in need of maintenance and repair, instead accumulating in the Z-line region (Figures 3A and 3B). In zebrafish, it has been shown that the Z-line holds a "reservoir" of UNC-45B, which shuttles to the myosin-containing A-band of the muscle sarcomere in response to eccentric exercise or induced damage to the myofiber.[51,52] This abnormal localization was observed in all three analyzed samples and, thus, seems independent of the underlying variant and UNC-45B domain impacted. Even though a biopsy provides only a static image, the abnormal localization is consistent with the assumption that the dynamic shuttling process might be impaired as well. Lack of proper UNC-45B localization and function under conditions of continued sarcomere use and stress could conceivably lead to the multifocal disruption and ultimate disarray of the myofibrillar apparatus, corresponding to the histologic and ultrastructural findings of eccentric and unstructured cores seen in our affected individuals. This might also help explain why the myopathic phenotype seen in *UNC45B*-related disease shows a progressive course distinct from the typical more static clinical course of congenital myopathies. Further *in vitro* testing will be required to determine whether the mislocalized UNC-45B observed in the affected individual's muscle impairs the recurring myosin cross-bridge cycling needed for repeated contraction.

Previous work on the highly conserved UNC-45 in various models including *C. elegans*, zebrafish, and mice, has shown that loss of UNC-45 is embryonically lethal.[29,30,53] In this context, it is notable that we have not observed individuals with bi-allelic null variants, and no homozygous null variants are listed in gnomAD, suggesting that this situation in the human may also be either not tolerated or be associated with a considerably more severe phenotype. We have shown that the recurring c.2261G>A variant is a complex splice allele that creates a hypomorph scenario, with the residual protein containing the p.Arg754Gln variant. This conclusion is supported by analysis of available UNC-45B muscle biopsies because all analyzed samples had a reduction in UNC-45B by

(C) Population motility of 60 young adult *unc-45(m94)* worms expressing the indicated UNC-45 variants on a 24-well plate filled with NGM and seeded with OP50 was measured with the ARENA WMicrotracker system (NemaMetrix) at 25°C for 24 h after reaching adulthood. Motility data was binned in 15 min time buckets before plotting for easier interpretability.
(D) Phalloidin-staining of F-actin-containing I-bands in *unc-45(m94)* mutant worms expressing the indicated UNC-45 variants.
(E) The number of I-bands is given per body wall muscle cell (indicated by dashed white line in [D]), with all 12 analyzed cells located in the same area between pharynx and vulva. *$p < 0.005$ compared to control in non-parametric Kruskal-Wallis test.
(F) Co-immunoprecipitation of myosin heavy chain B (MHC B) and Hsp90 (DAF-21) from cell lysates of *unc-45(m94)* mutant worms expressing the indicated FLAG-tagged UNC-45 variants grown at 25°C. Representative result of one of three experiments is shown.

immunoblot, which was most significant in the homozygous c.2261G>A biopsy (Figure 4C). Thus, we suspect that the disease mechanisms for this variant are largely driven by the protein deficiency, with additional contribution from a functionally impaired residual protein. Recombinant UNC-45B (p.Arg754Gln) variant protein indeed exhibited a lower melting temperature in thermal shift assays and aggregation tendency (Figures 5D and 5E). On the other hand, the ability of the corresponding *C. elegans* variant UNC-45 (p.Arg767Gln) to rescue a temperature-sensitive mutant allele in transgenic rescue assays corroborates the notion that the reduction in overall protein amount is the cause for the disease phenotype rather than the missense and possibly impaired residual protein itself (Figure 6).

In supplemental *C. elegans* biochemical assays, no changes in UNC-45 ubiquitylation were detected (Figure S4C), although both UCS domain missense variants were slightly more susceptible to trypsin proteolysis (Figures S4D and S4E). The UNC-45 transgenes of p.Arg778Trp (*C. elegans* p.Arg792Trp), of p.Ser403Pro (*C. elegans* p.Ile422Pro), and of p.Cys514Arg (*C. elegans* p.Cys532Arg) were found to have a more detrimental effect on function, with an inadequate rescue of the paralyzed phenotype and impaired binding to myosin for p.Arg778Trp. These more severe and obvious functional consequences in the *C. elegans* rescue assay are consistent with the fact that the variants cause disease in the human situation. Therefore, we propose that *UNC45B* variants impact UNC-45B chaperone activity through a reduction in overall protein levels (c.2261G>A), impaired normal myosin-binding (c.2332C>T [p.Arg778Trp]), or a combination of both.

UNC45B-related disease can be classified as both a chaperonopathy resulting in a secondary myosinopathy as well as a myofibrillar dystrophy, given the progressive disintegration of the myofibrillar apparatus. The continued dissolution of the myofibrillar structure, which clinically manifests as progressive muscle weakness, is characteristic of the chaperone dysfunction in forms of childhood-onset dystrophy.[8] Pathologically, this disorder could be considered a myofibrillar dystrophy because the excessive nuclear centralization seen on histology is a marker of an activated regenerative process. This is in contrast to a sarcolemmal dystrophic process, which typically leads to a more inflammatory and fibrotic picture, leading to an excessive matrix and fat proliferation. In *UNC45B*-related disease, we suspect a "dystrophic process internal to the myofiber," causing fibers to disappear focally with less of matrix reaction, hence the marbled appearance on muscle MR imaging. Bi-allelic variants in *UNC45B* should therefore be considered in individuals presenting with a myopathy specifically in the presence of core histology and ultrastructural findings including cytoplasmic bodies, rods, and autophagic lesions. Additional research is needed to elucidate the exact pathogenic *UNC45B*-related disease mechanism further and to find therapeutic strategies to restore sarcomeric homeostasis through modulating chaperone activity. This has shown great promise for neurodegenerative disorders, with a specific interest in the finding that overexpression of UNC-45 in a *Drosophila* model of Huntington-induced cardiac amyloidosis resulted in reduced poly-glutamine aggregation and myofibrillar disorganization.[54] Taken together, our data solidify the role of UNC-45B as a key regulator of myofibril maintenance and function, a tightly regulated pathway that is conserved from human to yeast, impaired UNC-45B function results in recognizable muscle pathology clinically manifesting with myopathy.

Data and Code Availability

Sequence data that support the findings of this study have been deposited in dbGaP (https://www.ncbi.nlm.nih.gov/gap). All the other data supporting the findings of this study are available within the article and its supplementary information files and from the corresponding author upon reasonable request

Supplemental Data

Supplemental Data can be found online at https://doi.org/10.1016/j.ajhg.2020.11.002.

Acknowledgments

We thank the individuals and their families for participating in our research study and Christopher Mendoza, Christine Jones, Gilberto ("Mike") Averion, Rupleen Kaur, Kia Brooks, and Janelle Geist Hauserman for their help in the clinic and the laboratory. We would like to thank the CHUGA Molecular Biology facility platform for their help with exome sequencing. We thank Y. Kohara, the *Caenorhabditis* Genetics Center (funded by the NIH National Center for Research Resources), the Dana-Farber Cancer Institute, and Addgene and Geneservice for plasmids, cDNAs, and worm strains. We thank the CECAD Imaging facility for support with confocal microscopy. In particular, we thank Vishnu Balaji for the purification of LET-70-HIS and VSV-CHN-1-HIS proteins and help with *in vitro* studies. For the complete Acknowledgments including funding sources, please see Supplemental Information.

Declaration of Interests

The authors declare no competing interests.

Received: June 15, 2020
Accepted: November 3, 2020
Published: November 19, 2020

Web Resources

Genotype Tissue Expression (GTEx) Project, https://www.gtexportal.org/
gnomAD, https://gnomad.broadinstitute.org/
Online Mendelian Inheritance in Man, see https://www.omim.org
UCSC Genome Browser, http://genome.ucsc.edu/
UniProt database, https://www.uniprot.org/

References

1. Kim, J., Löwe, T., and Hoppe, T. (2008). Protein quality control gets muscle into shape. Trends Cell Biol. *18*, 264–272.
2. Vicart, P., Caron, A., Guicheney, P., Li, Z., Prévost, M.C., Faure, A., Chateau, D., Chapon, F., Tomé, F., Dupret, J.M., et al. (1998). A missense mutation in the alphaB-crystallin chaperone gene causes a desmin-related myopathy. Nat. Genet. *20*, 92–95.
3. Selcen, D., Muntoni, F., Burton, B.K., Pegoraro, E., Sewry, C., Bite, A.V., and Engel, A.G. (2009). Mutation in BAG3 causes severe dominant childhood muscular dystrophy. Ann. Neurol. *65*, 83–89.
4. Smith, D.A., Carland, C.R., Guo, Y., and Bernstein, S.I. (2014). Getting folded: chaperone proteins in muscle development, maintenance and disease. Anat. Rec. (Hoboken) *297*, 1637–1649.
5. Harms, M.B., Sommerville, R.B., Allred, P., Bell, S., Ma, D., Cooper, P., Lopate, G., Pestronk, A., Weihl, C.C., and Baloh, R.H. (2012). Exome sequencing reveals DNAJB6 mutations in dominantly-inherited myopathy. Ann. Neurol. *71*, 407–416.
6. Sarparanta, J., Jonson, P.H., Golzio, C., Sandell, S., Luque, H., Screen, M., McDonald, K., Stajich, J.M., Mahjneh, I., Vihola, A., et al. (2012). Mutations affecting the cytoplasmic functions of the co-chaperone DNAJB6 cause limb-girdle muscular dystrophy. Nat. Genet. *44*, 450–455.
7. Lupo, V., Aguado, C., Knecht, E., and Espinós, C. (2016). Chaperonopathies: Spotlight on Hereditary Motor Neuropathies. Front. Mol. Biosci. *3*, 81.
8. Weihl, C.C., Udd, B., Hanna, M.; and ENMC workshop study group (2018). 234th ENMC International Workshop: Chaperone dysfunction in muscle disease Naarden, The Netherlands, 8-10 December 2017. Neuromuscul. Disord. *28*, 1022–1030.
9. Clark, K., Langeslag, M., Figdor, C.G., and van Leeuwen, F.N. (2007). Myosin II and mechanotransduction: a balancing act. Trends Cell Biol. *17*, 178–186.
10. Wesche, S., Arnold, M., and Jansen, R.P. (2003). The UCS domain protein She4p binds to myosin motor domains and is essential for class I and class V myosin function. Curr. Biol. *13*, 715–724.
11. Toi, H., Fujimura-Kamada, K., Irie, K., Takai, Y., Todo, S., and Tanaka, K. (2003). She4p/Dim1p interacts with the motor domain of unconventional myosins in the budding yeast, Saccharomyces cerevisiae. Mol. Biol. Cell *14*, 2237–2249.
12. Srikakulam, R., and Winkelmann, D.A. (1999). Myosin II folding is mediated by a molecular chaperonin. J. Biol. Chem. *274*, 27265–27273.
13. Epstein, H.F., and Thomson, J.N. (1974). Temperature-sensitive mutation affecting myofilament assembly in Caenorhabditis elegans. Nature *250*, 579–580.
14. Lee, C.F., Melkani, G.C., and Bernstein, S.I. (2014). The UNC-45 myosin chaperone: from worms to flies to vertebrates. Int. Rev. Cell Mol. Biol. *313*, 103–144.
15. Price, M.G., Landsverk, M.L., Barral, J.M., and Epstein, H.F. (2002). Two mammalian UNC-45 isoforms are related to distinct cytoskeletal and muscle-specific functions. J. Cell Sci. *115*, 4013–4023.
16. Hellerschmied, D., Lehner, A., Franicevic, N., Arnese, R., Johnson, C., Vogel, A., Meinhart, A., Kurzbauer, R., Deszcz, L., Gazda, L., et al. (2019). Molecular features of the UNC-45 chaperone critical for binding and folding muscle myosin. Nat. Commun. *10*, 4781.
17. Gazda, L., Pokrzywa, W., Hellerschmied, D., Löwe, T., Forné, I., Mueller-Planitz, F., Hoppe, T., and Clausen, T. (2013). The myosin chaperone UNC-45 is organized in tandem modules to support myofilament formation in C. elegans. Cell *152*, 183–195.
18. Hoppe, T., Cassata, G., Barral, J.M., Springer, W., Hutagalung, A.H., Epstein, H.F., and Baumeister, R. (2004). Regulation of the myosin-directed chaperone UNC-45 by a novel E3/E4-multiubiquitylation complex in C. elegans. Cell *118*, 337–349.
19. Janiesch, P.C., Kim, J., Mouysset, J., Barikbin, R., Lochmüller, H., Cassata, G., Krause, S., and Hoppe, T. (2007). The ubiquitin-selective chaperone CDC-48/p97 links myosin assembly to human myopathy. Nat. Cell Biol. *9*, 379–390.
20. Sobreira, N., Schiettecatte, F., Valle, D., and Hamosh, A. (2015). GeneMatcher: a matching tool for connecting investigators with an interest in the same gene. Hum. Mutat. *36*, 928–930.
21. Waterhouse, A., Bertoni, M., Bienert, S., Studer, G., Tauriello, G., Gumienny, R., Heer, F.T., de Beer, T.A.P., Rempfer, C., Bordoli, L., et al. (2018). SWISS-MODEL: homology modelling of protein structures and complexes. Nucleic Acids Res. *46* (W1), W296–W303.
22. Sambrook, J., and Russell, D.W. (2001). Molecular cloning: a laboratory manual (Cold Spring Harbor, N.Y.: Cold Spring Harbor Laboratory Press).
23. Brenner, S. (1974). The genetics of Caenorhabditis elegans. Genetics *77*, 71–94.
24. Stiernagle, T. (2006). Maintenance of C. elegans. WormBook, 1–11.
25. Praitis, V., Casey, E., Collar, D., and Austin, J. (2001). Creation of low-copy integrated transgenic lines in Caenorhabditis elegans. Genetics *157*, 1217–1226.
26. Huxley, H.E. (1969). The mechanism of muscular contraction. Science *164*, 1356–1365.
27. Prill, K., Carlisle, C., Stannard, M., Windsor Reid, P.J., and Pilgrim, D.B. (2019). Myomesin is part of an integrity pathway that responds to sarcomere damage and disease. PLoS ONE *14*, e0224206.
28. Wohlgemuth, S.L., Crawford, B.D., and Pilgrim, D.B. (2007). The myosin co-chaperone UNC-45 is required for skeletal and cardiac muscle function in zebrafish. Dev. Biol. *303*, 483–492.
29. Etard, C., Behra, M., Fischer, N., Hutcheson, D., Geisler, R., and Strähle, U. (2007). The UCS factor Steif/Unc-45b interacts with the heat shock protein Hsp90a during myofibrillogenesis. Dev. Biol. *308*, 133–143.
30. Chen, D., Li, S., Singh, R., Spinette, S., Sedlmeier, R., and Epstein, H.F. (2012). Dual function of the UNC-45b chaperone with myosin and GATA4 in cardiac development. J. Cell Sci. *125*, 3893–3903.
31. Karczewski, K.J., Francioli, L.C., Tiao, G., Cummings, B.B., Alföldi, J., Wang, Q., Collins, R.L., Laricchia, K.M., Ganna, A., Birnbaum, D.P., et al.; Genome Aggregation Database Consortium (2020). The mutational constraint spectrum quantified from variation in 141,456 humans. Nature *581*, 434–443.
32. Zhang, S., Samocha, K.E., Rivas, M.A., Karczewski, K.J., Daly, E., Schmandt, B., Neale, B.M., MacArthur, D.G., and Daly, M.J. (2018). Base-specific mutational intolerance near splice sites clarifies the role of nonessential splice nucleotides. Genome Res. *28*, 968–974.

33. Rivas, M.A., Pirinen, M., Conrad, D.F., Lek, M., Tsang, E.K., Karczewski, K.J., Maller, J.B., Kukurba, K.R., DeLuca, D.S., Fromer, M., et al.; GTEx Consortium; and Geuvadis Consortium (2015). Human genomics. Effect of predicted protein-truncating genetic variants on the human transcriptome. Science *348*, 666–669.
34. Barral, J.M., Hutagalung, A.H., Brinker, A., Hartl, F.U., and Epstein, H.F. (2002). Role of the myosin assembly protein UNC-45 as a molecular chaperone for myosin. Science *295*, 669–671.
35. Gieseler, K., Qadota, H., and Benian, G.M. (2017). Development, structure, and maintenance of C. elegans body wall muscle. WormBook *2017*, 1–59.
36. Landsverk, M.L., Li, S., Hutagalung, A.H., Najafov, A., Hoppe, T., Barral, J.M., and Epstein, H.F. (2007). The UNC-45 chaperone mediates sarcomere assembly through myosin degradation in Caenorhabditis elegans. J. Cell Biol. *177*, 205–210.
37. Nicholls, P., Bujalowski, P.J., Epstein, H.F., Boehning, D.F., Barral, J.M., and Oberhauser, A.F. (2014). Chaperone-mediated reversible inhibition of the sarcomeric myosin power stroke. FEBS Lett. *588*, 3977–3981.
38. Dafsari, H.S., Kocaturk, N.M., Daimagüler, H.S., Brunn, A., Dötsch, J., Weis, J., Deckert, M., and Cirak, S. (2019). Bi-allelic mutations in uncoordinated mutant number-45 myosin chaperone B are a cause for congenital myopathy. Acta Neuropathol. Commun. *7*, 211.
39. Amburgey, K., McNamara, N., Bennett, L.R., McCormick, M.E., Acsadi, G., and Dowling, J.J. (2011). Prevalence of congenital myopathies in a representative pediatric united states population. Ann. Neurol. *70*, 662–665.
40. Nance, J.R., Dowling, J.J., Gibbs, E.M., and Bönnemann, C.G. (2012). Congenital myopathies: an update. Curr. Neurol. Neurosci. Rep. *12*, 165–174.
41. Schartner, V., Romero, N.B., Donkervoort, S., Treves, S., Munot, P., Pierson, T.M., Dabaj, I., Malfatti, E., Zaharieva, I.T., Zorzato, F., et al. (2017). Dihydropyridine receptor (DHPR, CACNA1S) congenital myopathy. Acta Neuropathol. *133*, 517–533.
42. Jungbluth, H., Müller, C.R., Halliger-Keller, B., Brockington, M., Brown, S.C., Feng, L., Chattopadhyay, A., Mercuri, E., Manzur, A.Y., Ferreiro, A., et al. (2002). Autosomal recessive inheritance of RYR1 mutations in a congenital myopathy with cores. Neurology *59*, 284–287.
43. Agrawal, P.B., Pierson, C.R., Joshi, M., Liu, X., Ravenscroft, G., Moghadaszadeh, B., Talabere, T., Viola, M., Swanson, L.C., Haliloğlu, G., et al. (2014). SPEG interacts with myotubularin, and its deficiency causes centronuclear myopathy with dilated cardiomyopathy. Am. J. Hum. Genet. *95*, 218–226.
44. Geach, T.J., and Zimmerman, L.B. (2010). Paralysis and delayed Z-disc formation in the Xenopus tropicalis unc45b mutant dicky ticker. BMC Dev. Biol. *10*, 75.
45. Melkani, G.C., Bodmer, R., Ocorr, K., and Bernstein, S.I. (2011). The UNC-45 chaperone is critical for establishing myosin-based myofibrillar organization and cardiac contractility in the Drosophila heart model. PLoS ONE *6*, e22579.
46. Lossos, A., Oldfors, A., Fellig, Y., Meiner, V., Argov, Z., and Tajsharghi, H. (2013). MYH2 mutation in recessive myopathy with external ophthalmoplegia linked to chromosome 17p13.1-p12. Brain *136*, e238.
47. Tajsharghi, H., Oldfors, A., Macleod, D.P., and Swash, M. (2007). Homozygous mutation in MYH7 in myosin storage myopathy and cardiomyopathy. Neurology *68*, 962.
48. Saade, D.N., Neuhaus, S.B., Foley, A.R., and Bönnemann, C.G. (2019). The Use of Muscle Ultrasound in the Diagnosis and Differential Diagnosis of Congenital Disorders of Muscle in the Age of Next Generation Genetics. Semin. Pediatr. Neurol. *29*, 44–54.
49. Warman Chardon, J., and Straub, V. (2017). The Role of Muscle Imaging in the Diagnosis and Assessment of Children with Genetic Muscle Disease. Neuropediatrics *48*, 233–241.
50. Foley, A.R., Donkervoort, S., and Bönnemann, C.G. (2015). Next-generation sequencing still needs our generation's clinicians. Neurol. Genet. *1*, e13.
51. Etard, C., Roostalu, U., and Strähle, U. (2008). Shuttling of the chaperones Unc45b and Hsp90a between the A band and the Z line of the myofibril. J. Cell Biol. *180*, 1163–1175.
52. Lee, C.F., Melkani, G.C., Yu, Q., Suggs, J.A., Kronert, W.A., Suzuki, Y., Hipolito, L., Price, M.G., Epstein, H.F., and Bernstein, S.I. (2011). Drosophila UNC-45 accumulates in embryonic blastoderm and in muscles, and is essential for muscle myosin stability. J. Cell Sci. *124*, 699–705.
53. Venolia, L., and Waterston, R.H. (1990). The unc-45 gene of Caenorhabditis elegans is an essential muscle-affecting gene with maternal expression. Genetics *126*, 345–353.
54. Melkani, G.C., Trujillo, A.S., Ramos, R., Bodmer, R., Bernstein, S.I., and Ocorr, K. (2013). Huntington's disease induced cardiac amyloidosis is reversed by modulating protein folding and oxidative stress pathways in the Drosophila heart. PLoS Genet. *9*, e1004024.

The American Journal of Human Genetics, Volume *107*

Supplemental Data

Pathogenic Variants in the Myosin Chaperone UNC-45B Cause Progressive Myopathy with Eccentric Cores

Sandra Donkervoort, Carl E. Kutzner, Ying Hu, Xavière Lornage, John Rendu, Tanya Stojkovic, Jonathan Baets, Sarah B. Neuhaus, Jantima Tanboon, Reza Maroofian, Véronique Bolduc, Magdalena Mroczek, Stefan Conijn, Nancy L. Kuntz, Ana Töpf, Soledad Monges, Fabiana Lubieniecki, Riley M. McCarty, Katherine R. Chao, Serena Governali, Johann Böhm, Kanokwan Boonyapisit, Edoardo Malfatti, Tumtip Sangruchi, Iren Horkayne-Szakaly, Carola Hedberg-Oldfors, Stephanie Efthymiou, Satoru Noguchi, Sarah Djeddi, Aritoshi Iida, Gabriella di Rosa, Chiara Fiorillo, Vincenzo Salpietro, Niklas Darin, Julien Fauré, Henry Houlden, Anders Oldfors, Ichizo Nishino, Willem de Ridder, Volker Straub, Wojciech Pokrzywa, Jocelyn Laporte, A. Reghan Foley, Norma B. Romero, Coen Ottenheijm, Thorsten Hoppe, and Carsten G. Bönnemann

Figure S1

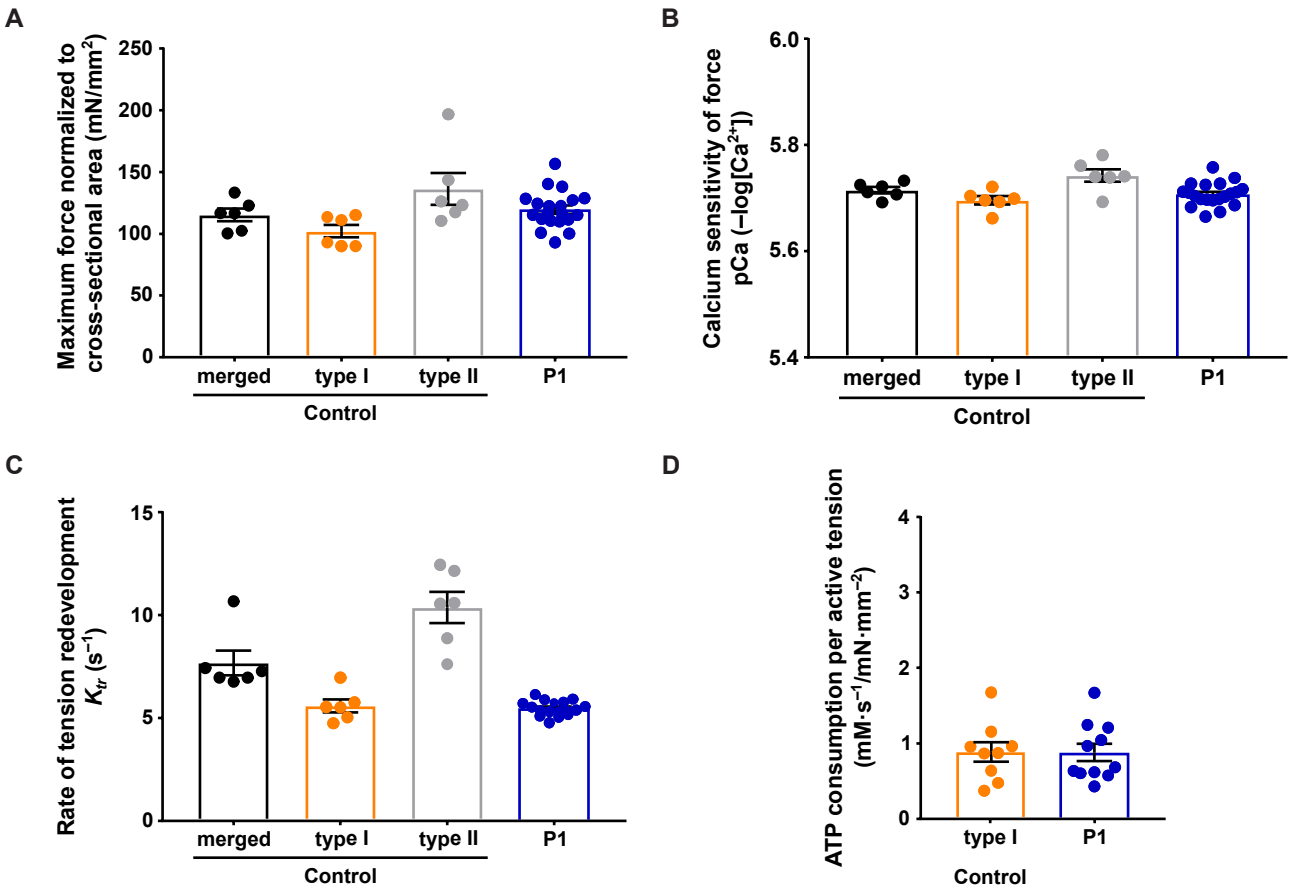
A
Maximum force normalized to cross-sectional area (mN/mm²)
250
200
150
100
50
0
merged
type I
type II
P1
Control
B
Calcium sensitivity of force pCa (–log[Ca²⁺])
6.0
5.8
5.6
5.4
merged
type I
type II
P1
Control
C
Rate of tension redevelopment K_{tr} (s⁻¹)
15
10
5
0
merged
type I
type II
P1
Control
D
ATP consumption per active tension (mM·s⁻¹/mN·mm⁻²)
4
3
2
1
0
type I
P1
Control

Figure S2

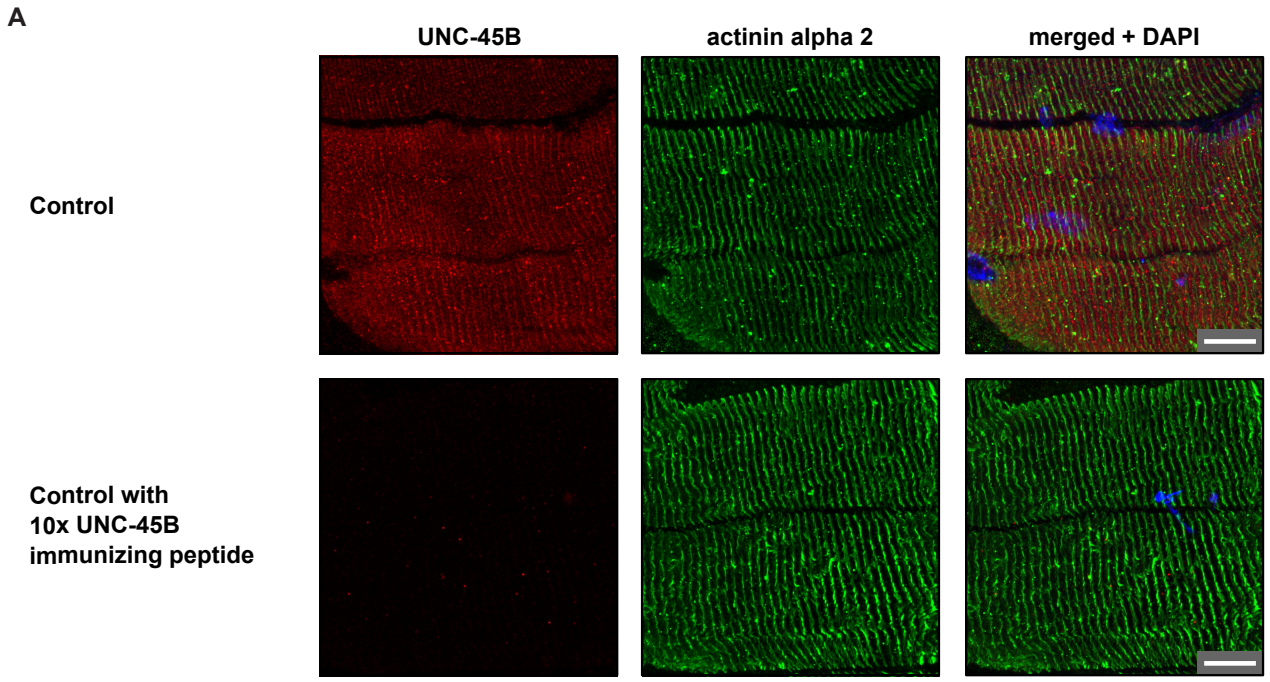
A
UNC-45B
actinin alpha 2
merged + DAPI
Control
Control with
10x UNC-45B
immunizing peptide

Figure S3

A

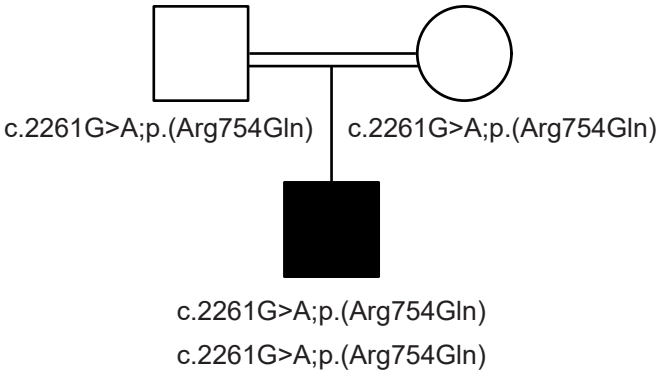

B

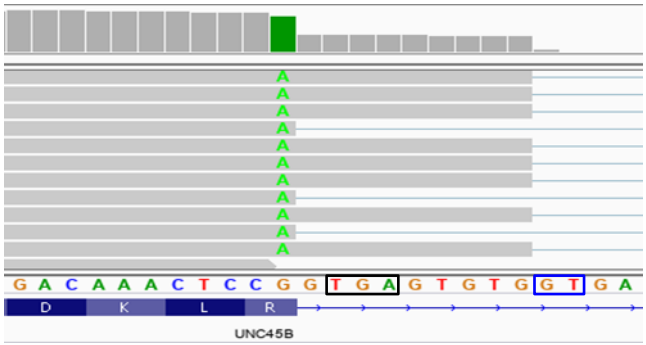

C

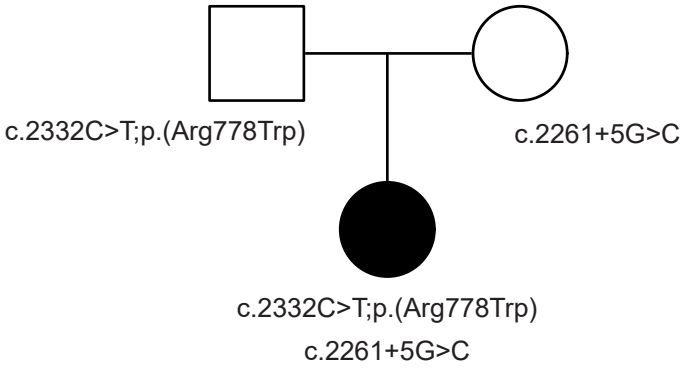

D

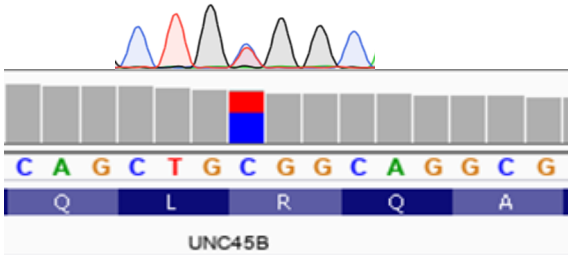

E

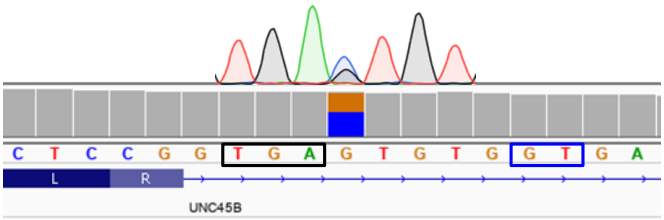

F

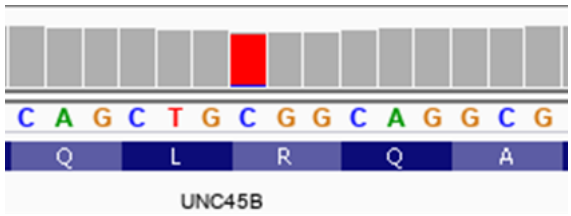

G

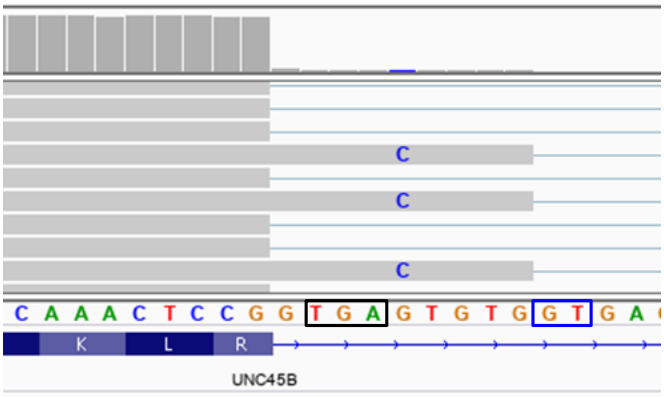

H

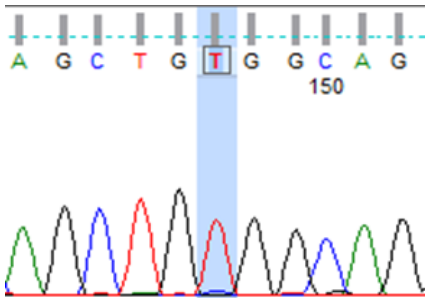

Figure S4

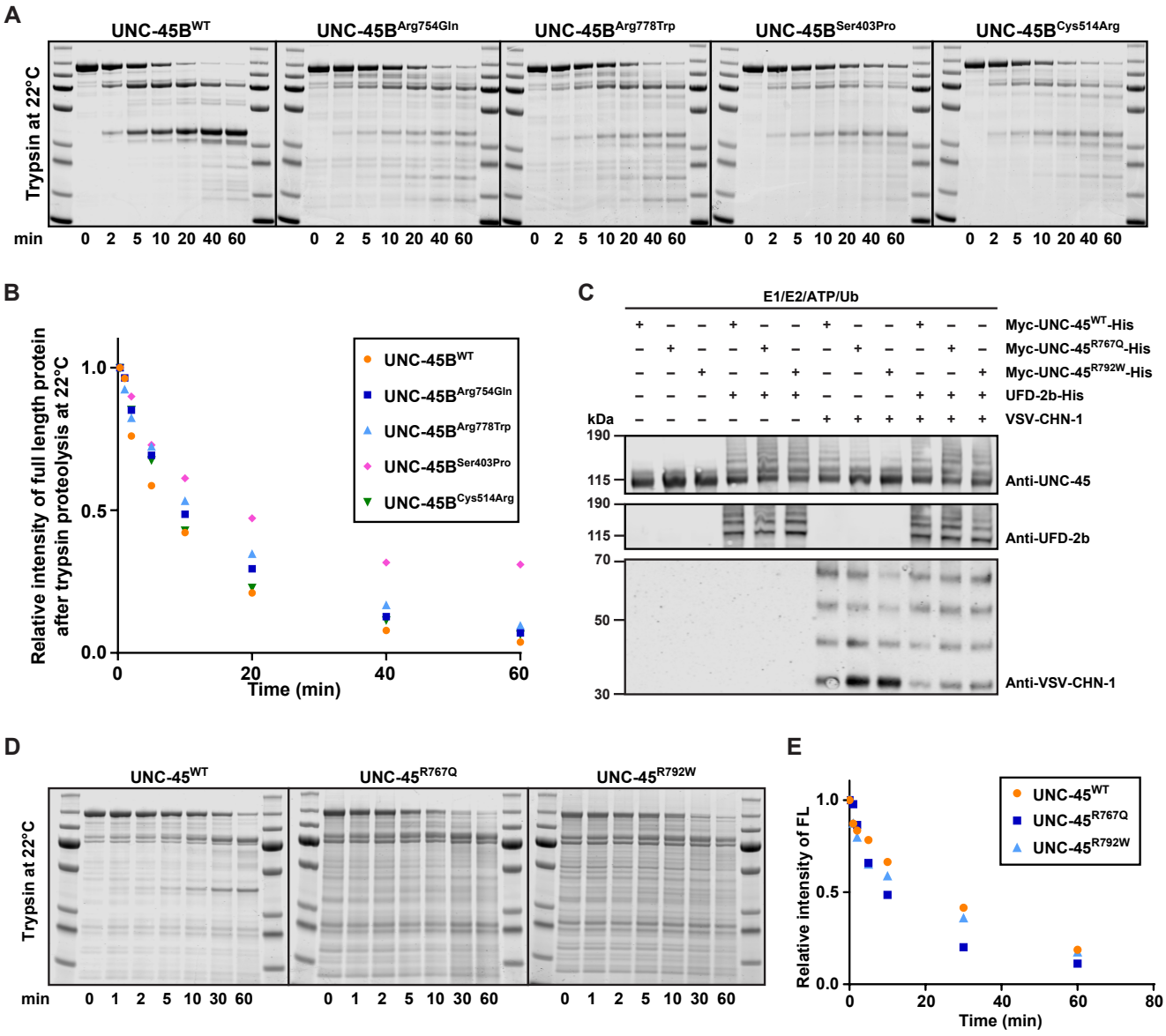
A
UNC-45B^WT
UNC-45B^Arg754Gln
UNC-45B^Arg778Trp
UNC-45B^Ser403Pro
UNC-45B^Cys514Arg
Trypsin at 22°C
min
0 2 5 10 20 40 60
B
Relative intensity of full length protein after trypsin proteolysis at 22°C
1.0
0.5
0.0
0
20
40
60
Time (min)
UNC-45B^WT
UNC-45B^Arg754Gln
UNC-45B^Arg778Trp
UNC-45B^Ser403Pro
UNC-45B^Cys514Arg
C
E1/E2/ATP/Ub
Myc-UNC-45^WT-His
Myc-UNC-45^R767Q-His
Myc-UNC-45^R792W-His
UFD-2b-His
VSV-CHN-1
kDa
190
115
70
50
30
Anti-UNC-45
Anti-UFD-2b
Anti-VSV-CHN-1
D
UNC-45^WT
UNC-45^R767Q
UNC-45^R792W
Trypsin at 22°C
min
0 1 2 5 10 30 60
E
Relative intensity of FL
1.0
0.5
0.0
0
20
40
60
80
Time (min)
UNC-45^WT
UNC-45^R767Q
UNC-45^R792W

Supplemental Figure Legends

Figure S1. Normal fiber contractile performance in P1 UNC-45B muscle. Muscle fiber contractile property from P1 (homozygous c.2261G>A *UNC45B*) was compared to controls. (A) Maximal tension generated by P1 fibers was similar to controls. (B) The calcium sensitivity of force was normal in P1 muscle compared to control. (C) Actin-myosin cross bridge attachment rates (K_{tr}) were normal in P1 muscle compared to type I control fibers, (D) with normal tension costs. Each data point in control bars represents the average of 8–15 muscle fibers from one control subject; each data point in P1 bar is one muscle fiber.

Figure S2. UNC-45B antibody is specific for the UNC-45B protein. (A) Longitudinal sections of control muscle biopsy incubated with either no UNC-45B immunizing peptide (top) or 10x excess of UNC-45B immunizing peptide (bottom), and stained for UNC-45B (red) and Z-disk protein α-actinin (green) confirmed the specificity of the UNC-45B antibody for the UNC-45B protein. Scale bar corresponds to 10 μm.

Figure S3. *UNC45B* pathogenic variants identified by exome sequencing. (A) Pedigree of P3. (B) BAM files visualized in Integrative Genomics Viewer (IGV) showing aligned P3 muscle RNA sequence reads from the homozygous c.2261G>A; p.(Arg754Gln) *UNC45B* variant. (C) Pedigree of P2. (D) Sanger Sequencing on P2 genomic DNA showing the c.2332C>T; p.(Arg778Trp) *UNC45B* variant (top) and BAM files visualized in Integrative Genomics Viewer (IGV) showing aligned sequence reads (bottom). (E) Sanger Sequencing on P2 genomic DNA showing the c.2261+5G>C

UNC45B variant (top) and BAM files visualized in IGV showing aligned sequence reads (bottom). (F) BAM files visualized in IGV showing aligned P2 muscle RNA sequence reads at the c.2332C>T; p.(Arg778Trp) *UNC45B* variant and revealing allelic imbalance in favor of the p.(Arg778Trp) variant. (G) BAM files visualized in IGV showing aligned P2 muscle RNA sequence reads of the c.2261+5G>C *UNC45B* variant and revealing the activation of a nearby intronic cryptic donor site which elongates the splice product to include an in-frame STOP codon. (H) Sequencing of reverse transcribed mRNA showing allelic imbalance towards the p.(Arg778Trp) variant.

Figure S4. *In vitro* analysis of human UNC-45B mutant proteins and *C. elegans* UNC-45 orthologue proteins. (A) Purified UNC-45B^{WT}, UNC-45B^{Arg754Gln}, UNC-45B^{Arg778Trp}, UNC-45B^{Ser403Pro}, and UNC-45B^{Cys514Arg} buffered solutions were subjected to partial proteolysis with trypsin at room temperature (22°C) and samples were loaded on SDS-PAGE gels for separation. Coomassie-stained gels are shown. (B) Quantification of full-length protein (FL, ~109 kDa) compared to time point 0 at 22°C. Results of three experiments. (C) *In vitro* ubiquitylation of purified UNC-45 wild-type and mutant proteins with the combination of enzymes indicated. The reaction was terminated by addition of SDS-PAGE sample buffer and analyzed by western blotting against UNC-45, UFD-2 and VSV-tagged CHN-1. (D) Purified *C. elegans* UNC-45^{WT}, UNC-45^{Arg767Gln}, and UNC-45^{Arg792Trp} solutions were subjected to partial proteolysis with trypsin at room temperature and samples were loaded on SDS-PAGE gels for separation. Coomassie stained gels are shown. (E) Quantification of full-length protein (FL, 109 kDa) compared to time point 0. Results of three independent experiments.

Supplemental Tables

Table S1. *UNC45B* variants identified.

DNA variant	RNA variant	Protein variant	*C. elegans* orthologous proteins
c.1207T>C	na	p.(Ser403Pro)	p.(Ile422Pro)
c.1540T>C	na	p.(Cys514Arg)	p.(Cys532Arg)
c.2261G>A	r.[2261g>a,2261_2262ins2261+1_2261+9]	p.(Arg754Gln), p.(Arg754GlnfsTer2)	p.(Arg767Gln)
c.2261+5G>C	r.2261_2262ins2261+1_2261+9	p.(Arg754GlnfsTer2)	p.(Arg767Gln)
c.2332C>T	r.2232c>u	p.(Arg778Trp)	p.(Arg792Trp)

Table S2. Oligonucleotides used in this study.

Name	5‘-3‘ sequence	Source
UNC-45B cDNA into pET21a FOR	gaagatctgATGGCAGAGGTGGAAGCG	This study
UNC-45B cDNA into pET21a REV	tggtggtgAGACACTGGTTTAATGAAACCATAATCCAT	This study
UNC-45B cDNA into pET21a vector FOR	CAGTGTCTcaccaccaccaccaccacta	This study
UNC-45B cDNA into pET21a vector REV	CTCTGCCATcagatcttcttcagaaataagtttttgttcc	This study
UNC-45B Arg754Gln mutagenesis FOR	GACAAACTCCaGCAGAAGATCTTTAAGGAG	This study
UNC-45B Arg754Gln mutagenesis REV	ACTCCGCCCAGACAGGTT	This study
UNC-45B Arg778Trp mutagenesis FOR	TGATCAGCTGtGGCAGGCGGC	This study
UNC-45B Arg778Trp mutagenesis REV	TGATTCTCAAACATGTAGTTCTCGATGTCTGG	This study
UNC-45B Ser403Pro mutagenesis FOR	CCAGACAGTGcCAGGGATCCT	This study
UNC-45B Ser403Pro mutagenesis REV	ATGGCATTCAAGTTCTTGTC	This study
UNC-45B Cys514Arg mutagenesis FOR	GGCCAAACAGcGTCGCAAGTG	This study

Name	5‘-3‘ sequence	Source
UNC-45B Cys514Arg mutagenesis REV	AGTTTTTCTGTCGACCCTTC	This study
UNC-45 Arg767Gln mutagenesis FOR	GATTCGATTCagGGACGAATTTTGAAAGAGAAG	This study
UNC-45 Arg767Gln mutagenesis REV	ACTGACGCTTGCCAAGTT	This study
UNC-45 Arg792Trp mutagenesis FOR	CGAGCATTTGtggGCCGCCGCCG	This study
UNC-45 Arg792Trp mutagenesis REV	TGATCCGTCATAAACCAGAATTCCTCAATCTTTG	This study
UNC-45 Ile422Pro mutagenesis FOR	ATGCTTCTTGccTACAATGCTTCAAG	This study
UNC-45 Ile422Pro mutagenesis REV	GATAGTTTGATACGGTATTTG	This study
UNC-45 Cys532Arg mutagenesis FOR	GGCGAAGACTcGCAAGAAATTC	This study
UNC-45 Cys532Arg mutagenesis REV	AAACTGATCACTGCTTCTTC	This study
unc-45 genotyping FOR	AGATCAAGGCGGGACATGC	This study
unc-45(m94) genotyping REV in combination with EcoRI digestion	TCCACTCGATACTTGTTCGCTTTCT	This study
FLAG-tag genotyping REV in combination with BsmFI digestion for R767Q substitution or in combination with Sau96I digestion for R792W substitution	GTCATCGTCATCCTTGTAATC	This study

Table S3. *C. elegans* strains used in this study.

Strain name	Origin	Resource
C. elegans: Bristol (N2) strain as wild type (WT)	CGC	Wormbase ID: N2
unc-119(ed4)III	Baumeister Lab	BR854
unc-45(m94)III	CGC	Wormbase ID: DR94
unc-45(m94)III; hhIs84[unc-119(+); unc-54::unc-45^{FLAG}]	Hoppe Lab	Gazda et al., 2013
unc-45(m94)III; hhIs238[unc-119(+); unc-54::unc-45R767Q^{FLAG}]	this study	N/A
unc-45(m94)III; hhIs243[unc-119(+); unc-54::unc-45R792W^{FLAG}]	this study	N/A
unc-45(m94)III; hhIs254[unc-119(+); Punc-54::unc-45I422P^{FLAG}]	this study	N/A
unc-45(m94)III; hhIs253[unc-119(+); Punc-54::unc-45C532R^{FLAG}]	this study	N/A

Table S4. Relative fluorescence signal in partial trypsin proteolysis of recombinant UNC-45B mutant proteins at 37°C.

Time (min)	UNC-45B(WT)			
	1	2	MEAN	SD
0	1.00	1.00	1.00	0.00
1		0.88	0.88	
2	0.65	0.68	0.66	0.02
5	0.22	0.29	0.25	0.05
10	0.05	0.08	0.06	0.02
20	0.01	0.03	0.02	0.01
40	0.01	0.01	0.01	0.00
60	0.01	0.01	0.01	0.00

Time (min)	UNC-45B(Arg754Gln)				UNC-45B(Arg778Trp)			
	1	2	MEAN	SD	1	2	MEAN	SD
0	1.00	1.00	1.00	0.00	1.00	1.00	1.00	0.00
1		0.90	0.90			0.83	0.83	
2	0.68	0.74	0.71	0.04	0.62	0.70	0.66	0.06
5	0.32	0.48	0.40	0.11	0.32	0.40	0.36	0.05
10	0.20	0.34	0.27	0.09	0.20	0.31	0.26	0.08
20	0.19	0.28	0.24	0.07	0.13	0.24	0.19	0.08
40	0.15	0.25	0.20	0.07	0.15	0.13	0.14	0.02
60	0.12	0.10	0.11	0.01	0.08	0.25	0.17	0.12

Time (min)	UNC-45B(Ser403Pro)				UNC-45B(Cys514Arg)			
	1	2	MEAN	SD	1	2	MEAN	SD
0	1.00	1.00	1.00	0.00	1.00	1.00	1.00	0.00
1		0.98	0.98			0.93	0.93	
2	0.95	0.88	0.91	0.05	0.66	0.82	0.74	0.11
5	0.60	0.60	0.60	0.00	0.33	0.60	0.47	0.19
10	0.43	0.54	0.48	0.08	0.18	0.37	0.28	0.13
20	0.45	0.35	0.40	0.07	0.13	0.30	0.22	0.12
40	0.09	0.34	0.21	0.17	0.11	0.23	0.17	0.08
60	0.08	0.31	0.20	0.16	0.11	0.15	0.13	0.03

Table S5. Parameters of Boltzmann sigmoidal curve fit to normalized SYPRO fluorescence signals in thermal shift assay of recombinant UNC-45B mutant proteins.

	UNC45B^{WT}	UNC45B^{R754Q}	UNC45B^{R778W}	UNC45B^{S403P}	UNC45B^{C514R}
Boltzmann sigmoidal					
Best-fit values					
Bottom	= 0	= 0	= 0	= 0	= 0
Top	= 1	= 1	= 1	= 1	= 1
V50	43.16	38.18	37.85	37.88	36.9
Slope	1.58	1.324	1.464	1.274	1.742
Std. Error					
V50	0.04358	0.05145	0.04907	0.1241	0.03901
Slope	0.03976	0.04617	0.04361	0.1148	0.03492
95% CI (profile likelihood)					
V50	43.07 to 43.25	38.08 to 38.28	37.75 to 37.94	37.63 to 38.13	36.83 to 36.98
Slope	1.502 to 1.66	1.235 to 1.417	1.38 to 1.552	1.061 to 1.518	1.675 to 1.81
Goodness of Fit					
Degrees of Freedom	86	60	76	48	81
R square	0.9903	0.9852	0.9887	0.9061	0.9936
Absolute Sum of Squares	0.1025	0.1196	0.1248	0.5738	0.07059
Sy.x	0.03452	0.04465	0.04053	0.1093	0.02952
Constraints					
Bottom	Bottom = 0	Bottom = 0	Bottom = 0	Bottom = 0	Bottom = 0
Top	Top = 1	Top = 1	Top = 1	Top = 1	Top = 1
Number of points					
# of X values	123	123	123	114	123
# Y values analyzed	88	62	78	50	83

Table S6. Single normalized fluorescence values of thermal shift assays of recombinant UNC-45B mutant proteins.

Temperature (°C)	UNC-45B(WT)					UNC-45B(Arg754Gln)					UNC-45B(Arg778Trp)				
Replicate:	1	2	3	MEAN	SD	1	2	3	MEAN	SD	1	2	3	MEAN	SD
30.0															
30.5															
31.0											0.000000	0.032292	0.000000	0.010764	0.018644
31.5			0.000000	0.000000							0.000829	0.048511	0.000513	0.016618	0.027621
32.0			0.000104	0.000104							0.004261	0.065842	0.002395	0.024166	0.036105
32.5			0.000449	0.000449							0.010298	0.084136	0.005713	0.033382	0.044013
33.0			0.001122	0.001122							0.019768	0.103466	0.010571	0.044602	0.051185
33.5	0		0.002279	0.001140	0.001612	0.000000	0.084682	0.000000	0.028227	0.048891	0.034209	0.123759	0.017618	0.058529	0.057097
34.0	0.000896		0.004006	0.002451	0.002199	0.006790	0.105336	0.003368	0.038498	0.057909	0.055990	0.145756	0.028188	0.076645	0.061445
34.5	0.002740		0.006475	0.004608	0.002641	0.023173	0.128830	0.012009	0.054671	0.064466	0.086056	0.170197	0.044267	0.100173	0.064141
35.0	0.006060	0.000000	0.009842	0.005301	0.004965	0.052546	0.156110	0.028937	0.079198	0.067646	0.126776	0.198341	0.068555	0.131224	0.065007
35.5	0.011118	0.001725	0.014332	0.009058	0.006551	0.096974	0.189415	0.057609	0.114666	0.067661	0.179096	0.232780	0.103790	0.171889	0.064796
36.0	0.018021	0.005174	0.020065	0.014420	0.008072	0.157491	0.230120	0.100727	0.162779	0.064859	0.243016	0.274922	0.152094	0.223344	0.063734
36.5	0.026979	0.010693	0.027265	0.021646	0.009486	0.233210	0.279690	0.159532	0.224144	0.060590	0.316170	0.326915	0.213875	0.285653	0.062393
37.0	0.038360	0.018455	0.036089	0.030968	0.010896	0.322066	0.338296	0.233138	0.297834	0.056612	0.397254	0.387794	0.287630	0.357559	0.060745
37.5	0.052482	0.029148	0.046829	0.042820	0.012173	0.419336	0.404647	0.318488	0.380824	0.054482	0.482244	0.457117	0.370177	0.436513	0.058807
38.0	0.069396	0.042946	0.059641	0.057328	0.013376	0.519705	0.477022	0.410529	0.469085	0.055019	0.567708	0.531847	0.456794	0.518783	0.056599
38.5	0.089525	0.060021	0.074923	0.074823	0.014752	0.617565	0.551549	0.504387	0.557834	0.056850	0.650095	0.607984	0.543069	0.600383	0.053916
39.0	0.113394	0.080890	0.093053	0.095779	0.016423	0.708635	0.625301	0.595409	0.643115	0.058677	0.725852	0.682566	0.625103	0.677840	0.050541
39.5	0.141216	0.105381	0.114465	0.120354	0.018629	0.789225	0.695009	0.679695	0.721310	0.059313	0.793561	0.751666	0.700021	0.748416	0.046855
40.0	0.173464	0.134357	0.139761	0.149194	0.021191	0.857122	0.758348	0.754719	0.790063	0.058103	0.851089	0.813509	0.766112	0.810237	0.042583
40.5	0.210349	0.167989	0.169444	0.182594	0.024047	0.910849	0.814114	0.819729	0.848230	0.054302	0.897846	0.866390	0.823105	0.862447	0.037526
41.0	0.252556	0.206968	0.204289	0.221271	0.027126	0.951144	0.861618	0.873837	0.895533	0.048547	0.934422	0.909717	0.870895	0.905011	0.032024
41.5	0.300295	0.252328	0.244919	0.265848	0.030062	0.978745	0.901377	0.917531	0.932551	0.040813	0.962003	0.944156	0.909996	0.938718	0.026426
42.0	0.354042	0.305105	0.292197	0.317115	0.032624	0.994539	0.933735	0.951520	0.959931	0.031262	0.981297	0.970004	0.941502	0.964268	0.020508
42.5	0.414006	0.366161	0.346623	0.375597	0.034668	1.000000	0.959639	0.976336	0.978658	0.020281	0.993726	0.987409	0.966030	0.982389	0.014515
43.0	0.480135	0.436357	0.408717	0.441736	0.036012		0.979518	0.992378	0.985948	0.009093	1.000000	0.997408	0.983990	0.993799	0.008593
43.5	0.551691	0.514660	0.478200	0.514851	0.036746		0.993115	1.000000	0.996558	0.004868		1.000000	0.995519	0.997759	0.003169
44.0	0.627305	0.600207	0.553848	0.593787	0.037147		1.000000		1.000000				1.000000	1.000000	
44.5	0.704447	0.690238	0.633329	0.676005	0.037635										
45.0	0.779640	0.779062	0.713639	0.757447	0.037940										
45.5	0.849194	0.861676	0.790703	0.833858	0.037891										
46.0	0.909105	0.930666	0.860256	0.900009	0.036076										
46.5	0.955949	0.978786	0.918309	0.951014	0.030539										
47.0	0.986721	1.000000	0.961995	0.982905	0.019288										
47.5	1.000000		0.989432	0.994716	0.007472										
48.0			1.000000	1.000000											

Temperature (°C)	UNC-45B(Ser403Pro)					UNC-45B(Cys514Arg)				
Replicate:	1	2	3	MEAN	SD	1	2	3	MEAN	SD
30.0						0.000000	0.000000	0.000000	0.000000	0.000000
30.5						0.009974	0.016816	0.011468	0.012753	0.003598
31.0						0.022260	0.035468	0.024631	0.027453	0.007041
31.5						0.037123	0.056014	0.039488	0.044208	0.010292
32.0						0.055023	0.079129	0.056525	0.063559	0.013505
32.5						0.076161	0.105241	0.075939	0.085780	0.016854
33.0						0.100799	0.134043	0.098193	0.111012	0.019988
33.5	0.000000			0.000000		0.129797	0.166391	0.124254	0.140148	0.022896
34.0	0.003481			0.003481		0.164344	0.203265	0.154960	0.174190	0.025614
34.5	0.017108	0.242701	0.000000	0.086603	0.135455	0.204901	0.245093	0.190971	0.213655	0.028103
35.0	0.045554	0.277828	0.009984	0.111122	0.145463	0.252527	0.292546	0.233057	0.259376	0.030330
35.5	0.090113	0.319343	0.032158	0.147205	0.151866	0.307418	0.346848	0.281482	0.311916	0.032914
36.0	0.151482	0.368157	0.068011	0.195883	0.154921	0.368584	0.406959	0.335652	0.370398	0.035688
36.5	0.228367	0.429288	0.118128	0.258594	0.157767	0.434705	0.471901	0.394576	0.433728	0.038672
37.0	0.318679	0.499544	0.182054	0.333426	0.159258	0.504128	0.539779	0.457001	0.500303	0.041521
37.5	0.418938	0.577099	0.258688	0.418241	0.159207	0.574609	0.608573	0.521406	0.568196	0.043936
38.0	0.524070	0.659215	0.344852	0.509379	0.157696	0.643636	0.676512	0.585900	0.635349	0.045871
38.5	0.628804	0.740876	0.437500	0.602393	0.153403	0.709690	0.740659	0.649006	0.699785	0.046622
39.0	0.727770	0.816606	0.533001	0.692459	0.145063	0.770791	0.800220	0.709295	0.760102	0.046395
39.5	0.817088	0.883212	0.627140	0.775813	0.132932	0.825748	0.852871	0.765314	0.814645	0.044822
40.0	0.891387	0.937044	0.715573	0.848001	0.116936	0.873241	0.897695	0.815919	0.862285	0.041975
40.5	0.946588	0.974453	0.795449	0.905497	0.096317	0.912676	0.934385	0.860470	0.902510	0.037992
41.0	0.982693	0.995894	0.863978	0.947522	0.072651	0.943788	0.962453	0.898351	0.934864	0.032970
41.5	1.000000	1.000000	0.918957	0.972986	0.046790	0.967105	0.982633	0.929431	0.959723	0.027358
42.0			0.959803	0.959803		0.983222	0.994802	0.954238	0.977421	0.020895
42.5			0.986644	0.986644		0.993328	1.000000	0.973080	0.988803	0.014019
43.0			1.000000	1.000000		0.998679		0.986661	0.992670	0.008498
43.5						1.000000		0.995620	0.997810	0.003097
44.0								1.000000	1.000000	
44.5										
45.0										
45.5										
46.0										
46.5										
47.0										
47.5										
48.0										

Supplemental Methods

Whole Exome Sequencing

Trio WES for P1 and singleton WES for P5 was performed at the Broad Institute (Boston, USA) using Standard Germline Exome version 5, handled by the Genomics Platform's Core Exome/RNA product team. The process includes sample prep (Illumina Nextera), hybrid capture (Illumina Rapid Capture Enrichment 37Mb target), sequencing (Illumina, 150bp paired reads) and identification quality control check. The hybrid selection libraries typically meet or exceed 85% of targets at 20x, comparable to ~55x mean coverage.

Trio WES for P2 was performed using the SureSelect Human All Exon 50Mb capture library v5 (Agilent, Santa Clara, USA) and paired-end sequencing on Illumina HiSeq2500 (Illumina, San Diego, USA) with 30X coverage. The data were aligned to the GRCh37/hg19 reference genome, and variants were filtered according to their frequency in gnomAD (http://gnomad.broadinstitute.org/).

WES for P3 and P4 was performed using Nextera Flex for Enrichment library preparation (Illumina, San Diego, CA, USA). Libraries were sequenced using a NextSeq500 sequencer (Illumina, San Diego, CA, USA) with 150 bp paired-end reads. The reads were mapped to the human reference genome (GRCh37/hg19) by Burrows–Wheeler Aligner (BWA) bwa v0.7.17. Duplicate reads were removed with picard v2.2. On average, for P3 mean depth was 119X with 94.33% of regions covered at least 20X. For P4 mean depth was 101X with 93.5% of regions covered at least 20x. Variant calling was realized using the Genome Analysis Toolkit (GATK) v4.0.7.0 and annotated with Varaft 2V.16 [1].

WES for P6, P7 and P8 was performed using SureSelectXT Human All Exon V6 (Agilent Technologies, Santa Clara, CA, USA). Captured DNA was sequenced using a HiSeq 1000 (Illumina, San Diego, CA, USA) with 150 bp paired-end reads. The reads were mapped to the human reference genome (GRCh37/hg19) by Burrows–Wheeler Aligner (BWA) 0.7.5a-r405. Duplicate reads were removed with Picard 1.99. Variants were identified with the Genome Analysis Toolkit (GATK) v3.2 based on the GATK Best Practice Workflow and annotated with ANNOVAR (2017Jul16).

WES for P9 was performed as described elsewhere[2]. Briefly, target enrichment was performed with 2 µg genomic DNA using the SureSelectXT Human All Exon Kit V6 (Agilent Technologies, Santa Clara, CA, USA) to generate barcoded whole-exome sequencing libraries. Libraries were sequenced on the HiSeqX platform (Illumina, San Diego, CA, USA) with 50x coverage. Quality assessment of the sequence reads was performed by generating QC statistics with FastQC (http://www.bioinformatics.bbsrc.ac.uk/projects/fastqc). The bioinformatics filtering strategy included screening for only exonic and donor/acceptor splicing variants. In accordance with the pedigree and phenotype, priority was given to rare variants (<0.01% in public databases, including 1,000 Genomes project, NHLBI Exome Variant Server, Complete Genomics 69, and Exome Aggregation Consortium [ExAC v0.2]) that were fitting a recessive (homozygous or compound heterozygous) or a de novo model and/or variants in genes previously linked to proximal myopathy and other neurological disorders.

WES for P10 was performed by target enrichment on genomic DNA using the SureSelectXT Human All Exon V6 (Agilent Technologies, Santa Clara, CA, USA) and the

HiSeq2500 platform for sequencing (Illumina, San Diego, CA, USA). The paired-end reads were aligned to the reference genome (GRCh37/hg19) using the CLC Biomedical Genomics workbench (Qiagen, Hilden, Germany). On average, 90% of all regions were covered at least 7x. Data were analyzed using Ingenuity Variant Analysis (IVA) (Qiagen, Hilden, Germany).

Confirmation of variants and segregation was performed by Sanger sequencing.

RNA Sequencing

For P2, P3 and P4 muscle lysates were prepared with a Precellys 24 homogenizer (Bertin, Montigny-le-Bretonneux, France). RNA isolation and purification were performed using the TRI Reagent (MRC, Mongomery, USA), and paired-end sequenced on Illumina HiSeq2500 (Illumina, San Diego, USA). The data were aligned to the GRch38 reference genome. For splicing verifications, cDNA synthesis was performed with the SuperScript IV RT (Thermofischer, Waltham, USA) and amplified with *UNC45B*-specific primers.

Permeabilized muscle fiber mechanics

Single fibers were dissected from the muscle biopsies and permeabilized overnight as described previously[3]. This procedure renders the membranous structures in the muscle fibers permeable, which enables activation of the myofilaments with exogenous calcium. Preparations were washed thoroughly with relaxing solution and stored in 50% glycerol/relaxing solution at −20 °C. Single muscle fibers were dissected from the permeabilized strips, and were mounted using aluminum T-clips between a length motor (ASI 315C-I, Aurora Scientific Inc., Ontario, Canada) and a force transducer element (ASI

403A, Aurora Scientific Inc., Ontario, Canada) in a single fiber apparatus (ASI 802D, Aurora Scientific Inc., Ontario, Canada) that was mounted on the stage of an inverted microscope (Zeiss Axio Observer A1). Sarcomere length was determined using a high speed VSL camera and ASI 900B software (Aurora Scientific Inc., Ontario, Canada). Mechanical experiments were performed at a sarcomere length of 2.5 µm, to ensure that the sarcomeres operate at an optimal length (middle of the plateau phase). Fiber width and diameter were measured at three points along the fiber and the cross-sectional area was determined assuming an elliptical cross-section. The bathing solutions used during the experimental protocols were: a relaxing solution (100 mM BES, 6.97 mM EGTA, 6.48 mM $MgCl_2$, 5.89 mM Na_2-ATP, 40.76 mM K-propionate, 14.5 mM creatine phosphate), a pre-activating solution with low EGTA concentration (100 mM BES, 0.1 mM EGTA, 6.42 mM $MgCl_2$, 5.87 mM Na_2-ATP, 41.14 mM K-propionate, 14.5 mM creatine phosphate, 6.9 mM HDTA), and an activating solution (100 mM BES, 7.0 mM Ca-EGTA, 6.28 mM $MgCl_2$, 5.97 mM Na_2-ATP, 40.64 mM K-propionate, 14.5 mM creatine phosphate). The temperature of the bathing solutions was kept constant at 20°C using a TEC controller (ASI 825A, Aurora Scientific Inc. Ontario, Canada). The relaxation kinetics were calculated by fitting a mono-exponential through the force relaxation curve. To investigate the sarcomere-length dependency of force, maximal active tension was measured at incremental sarcomere lengths (2.0 – 3.5 µm).

To investigate submaximal force generating capacities at the sarcomere level, force-pCa relations were established. To determine the force-pCa relation (pCa = -log of molar free Ca^{2+} concentration), permeabilized muscle fibers were sequentially bathed in solutions with pCa values ranging from 4.5 to 9.0 and the steady-state force was measured. Force values were normalized to the maximal force obtained at pCa 4.5. The

obtained force-pCa data were fit to the Hill equation, providing the pCa_{50} and the Hill coefficient, n_H, an index of myofilament cooperativity.

To assess the tension cost during contraction, ATPase activity (temperature 12°C) at saturating [Ca^{2+}] (pCa 4.5) was measured photometrically by enzymatic coupling of the regeneration of ATP to the oxidation of NADH present in the bathing solution[4]. Sarcomere length was set at 2.5 µm. NADH breakdown was monitored via the absorption of near UV light at 340 nm. The activation buffer contained 10 mm phosphoenol pyruvate, with 4 mg•ml^{-1} pyruvate kinase (500 U•mg^{-1}), 0.24 mg•ml^{-1} lactate dehydrogenase (870 U•mg^{-1}) and 20 µm diadenosine-5′ pentaphosphate (A_2P_5). Briefly, the set up consisted of two anodized aluminium troughs (volume 80 µl each) containing relaxing and pre-activating solution and a measuring chamber (volume about 30 µl) containing activating solution. The solution was continuously stirred via a membrane at the base of the chamber. UV light passed through the chamber beneath the fibre, and the transmitted light was monitored by two UV-enhanced photodiodes at 340 and 400 nm. The photodiode at 400 nm provided a reference signal, independent of NADH concentration. A syringe, controlled by a stepper motor, was used to add 0.05 µl of 10 mM ADP at the end of each recording to calibrate the absorbance signal. Force during the enzymatic assay was measured by means of a strain gauge transducer (AE801 SensoNor, Horten, Norway). The force and the absorbance signals were filtered at 1 kHz and 2.5 Hz, respectively. The ATPase rate was measured as the slope over time of the absorbance signal. The ATPase rate was divided by tension (force/CSA) to determine the tension cost.

As the contractile properties of muscle fibers are influenced by the myosin heavy chain composition of the muscle fibers, we used a specialized SDS-PAGE technique to analyze the myosin heavy chain isoform composition in the muscle fibers used in

contractility experiments. In brief, muscle fibers were denatured by boiling for 2 minutes in SDS sample buffer. The stacking gel contained a 4% acrylamide concentration (pH 6.7), and the separating gel contained 7% acrylamide (pH 8.7) with 30% glycerol (v/v). The gels were run for 24h at 15 °C and a constant voltage of 275 volt. Finally, the gels were silver-stained, scanned, and analyzed with ImageQuant TL software (GE Healthcare, Chicago, IL).

Immunostaining & microscopy

Pre-cooled 100% methanol fixed 8 μm muscle longitudinal sections were blocked in PBS with 10% goat serum and 0.1% Tx-100, then incubated with primary antibodies anti-UNC-45B (HPA017861, Sigma) and anti-α-Actinin (A7811,sigma) with 10x of PrEST Antigen UNC-45B (APREST72666, Sigma) at 4°C overnight. The antibody labeling was detected with secondary antibodies Alexa 488- conjugated goat anti-mouse IgG and Alexa 568-conjugated goat anti-rabbit IgG (Thermofisher, Rockford, IL) for 1h at room temperature. Prepared muscle sections were imaged with a Zeiss Airy microscope (Zeiss, Germany).

In vitro ubiquitylation assay

Briefly, *C. elegans* UNC-45 recombinant proteins were incubated with *C. elegans* CHN-1 and UFD-2b recombinant proteins and the extent of ubiquitylation was evaluated in a western blot. Reactions were done in ubiquitinylation buffer (Enzo), supplemented with 1x ATP Regeneration Buffer (Enzo) and 50 μM ubiquitin (Flag-tagged, Boston Biochem). Ubiquitin activating enzyme E1 (His-tagged, Enzo) was used at a concentration of 0.1 μM. Enzyme E2 (LET-70-6xHIS), VSV-CHN-1-6xHIS and UFD-2b-6xHIS were purified in-house via HIS-binding to HisTrap FF columns on an ÄKTApurifier (GE Healthcare) or to

Ni-NTA agarose (QIAGEN). E2, E3 and substrate proteins were used at a concentration of 0.2 µM. After incubation at 30°C for 2 h, reactions were stopped by addition of 2x SDS-PAGE sample buffer (125 mM Tris pH 6.8, 4 % SDS, 20 % glycerol, 0.03 % bromophenol blue, 0.05 % β-mercaptoethanol) and boiling at 95°C for 5 min. Samples were run on 4-12% Bis-Tris gels (Invitrogen), transferred to nitrocellulose membranes, probed with antibodies for *C. elegans* UNC-45, UFD-2b (Biogenes) and VSV-tagged CHN-1 (P5D4, Roche), and detected using IRDye@ 800CW Goat anti-Mouse IgG secondary antibodies (LI-COR Biotechnology) on an Odyssey CLx Imager (LI-COR Biotechnology).

References

1. Desvignes, J.P., Bartoli, M., Delague, V., Krahn, M., Miltgen, M., Beroud, C., and Salgado, D. (2018). VarAFT: a variant annotation and filtration system for human next generation sequencing data. Nucleic Acids Res 46, W545-W553.
2. Mencacci, N.E., Kamsteeg, E.J., Nakashima, K., R'Bibo, L., Lynch, D.S., Balint, B., Willemsen, M.A., Adams, M.E., Wiethoff, S., Suzuki, K., et al. (2016). De Novo Mutations in PDE10A Cause Childhood-Onset Chorea with Bilateral Striatal Lesions. Am J Hum Genet 98, 763-771.
3. de Winter, J.M., Molenaar, J.P., Yuen, M., van der Pijl, R., Shen, S., Conijn, S., van de Locht, M., Willigenburg, M., Bogaards, S.J., van Kleef, E.S., et al. (2020). KBTBD13 is an actin-binding protein that modulates muscle kinetics. The Journal of clinical investigation 130, 754-767.
4. Ottenheijm, C.A., Lawlor, M.W., Stienen, G.J., Granzier, H., and Beggs, A.H. (2011). Changes in cross-bridge cycling underlie muscle weakness in patients with tropomyosin 3-based myopathy. Hum Mol Genet 20, 2015-2025.

Supplemental Acknowledgements

This research was supported (in part) by the Intramural Research Program of the NIH, NINDS to CGB and by the Deutsche Forschungsgemeinschaft (DFG) (FOR2743 and CECAD) to TH, DFG (FOR2743) and the European Molecular Biology Organization (EMBO) (Installation Grant No. 3916) to WP. Sequencing and analysis were provided by the Broad Institute of MIT and Harvard Center for Mendelian Genomics (Broad CMG) and was funded by the National Human Genome Research Institute,

the National Eye Institute, and the National Heart, Lung and Blood Institute grant UM1 HG008900 and in part by National Human Genome Research Institute grant R01 HG009141. Family P9 was collected as part of the SYNaPS Study Group collaboration funded by The Wellcome Trust and strategic award (Synaptopathies) funding (WT093205 MA and WT104033AIA). This research was conducted as part of the Queen Square Genomics group at University College London, supported by the National Institute for Health Research University College London Hospitals Biomedical Research Centre. This study was partially supported by the Intramural Research Grant (29-4 to NI; 30-9 to SN, AI) for Neurological and Psychiatric Disorders of NCNP; and by AMED under Grant Numbers JP19ek0109285h0003 and Joint Usage and Joint Research Programs, the Institute of Advanced Medical Sciences, Tokushima University (2019, A9 to AI). This work was supported by the Association Belge contre les Maladies Neuromusculaire (ABMM) and the EU Horizon 2020 program (Solve-RD). JB is supported by a Senior Clinical Researcher mandate of the Research Fund - Flanders (FWO). Authors of this publication are member of the European Reference Network for Rare Neuromuscular Diseases (ERN EURO-NMD) and of the European Reference Network for Rare Neurological Diseases (ERN-RND).This work was supported by the France Génomique National infrastructure, funded as part of the «Investissements d'Avenir» program managed by the Agence Nationale pour la Recherche (ANR-10-INBS-09), and by Fondation Maladies Rares within the frame of the "Myocapture" sequencing project.

The American Journal of Human Genetics, Volume *107*

Supplemental Data

Pathogenic Variants in the Myosin Chaperone UNC-45B Cause Progressive Myopathy with Eccentric Cores

Sandra Donkervoort, Carl E. Kutzner, Ying Hu, Xavière Lornage, John Rendu, Tanya Stojkovic, Jonathan Baets, Sarah B. Neuhaus, Jantima Tanboon, Reza Maroofian, Véronique Bolduc, Magdalena Mroczek, Stefan Conijn, Nancy L. Kuntz, Ana Töpf, Soledad Monges, Fabiana Lubieniecki, Riley M. McCarty, Katherine R. Chao, Serena Governali, Johann Böhm, Kanokwan Boonyapisit, Edoardo Malfatti, Tumtip Sangruchi, Iren Horkayne-Szakaly, Carola Hedberg-Oldfors, Stephanie Efthymiou, Satoru Noguchi, Sarah Djeddi, Aritoshi Iida, Gabriella di Rosa, Chiara Fiorillo, Vincenzo Salpietro, Niklas Darin, Julien Fauré, Henry Houlden, Anders Oldfors, Ichizo Nishino, Willem de Ridder, Volker Straub, Wojciech Pokrzywa, Jocelyn Laporte, A. Reghan Foley, Norma B. Romero, Coen Ottenheijm, Thorsten Hoppe, and Carsten G. Bönnemann

Figure S1

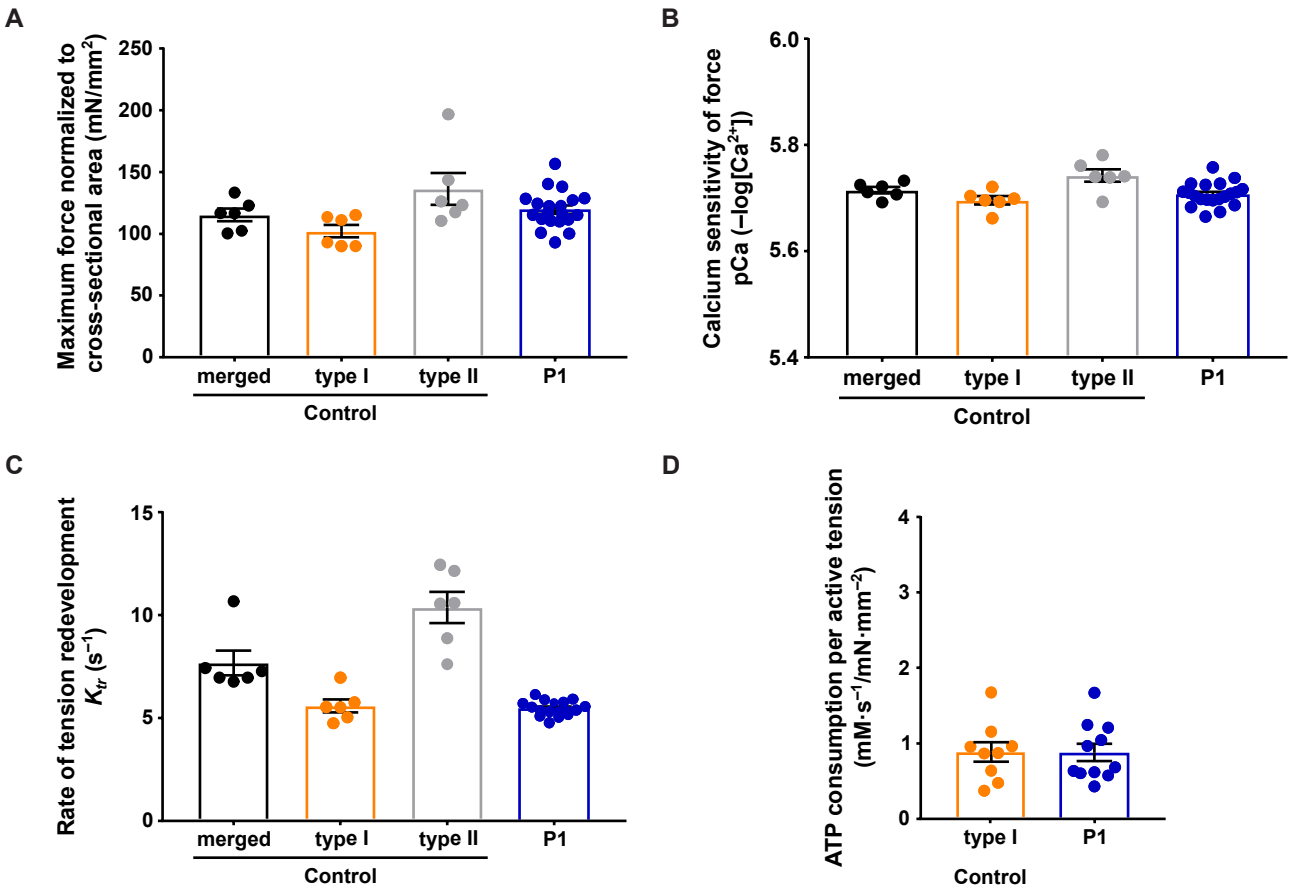
A
Maximum force normalized to cross-sectional area (mN/mm²)
250
200
150
100
50
0
merged
type I
type II
P1
Control
B
Calcium sensitivity of force pCa (–log[Ca²⁺])
6.0
5.8
5.6
5.4
merged
type I
type II
P1
Control
C
Rate of tension redevelopment K_{tr} (s⁻¹)
15
10
5
0
merged
type I
type II
P1
Control
D
ATP consumption per active tension (mM·s⁻¹/mN·mm⁻²)
4
3
2
1
0
type I
P1
Control

Figure S2

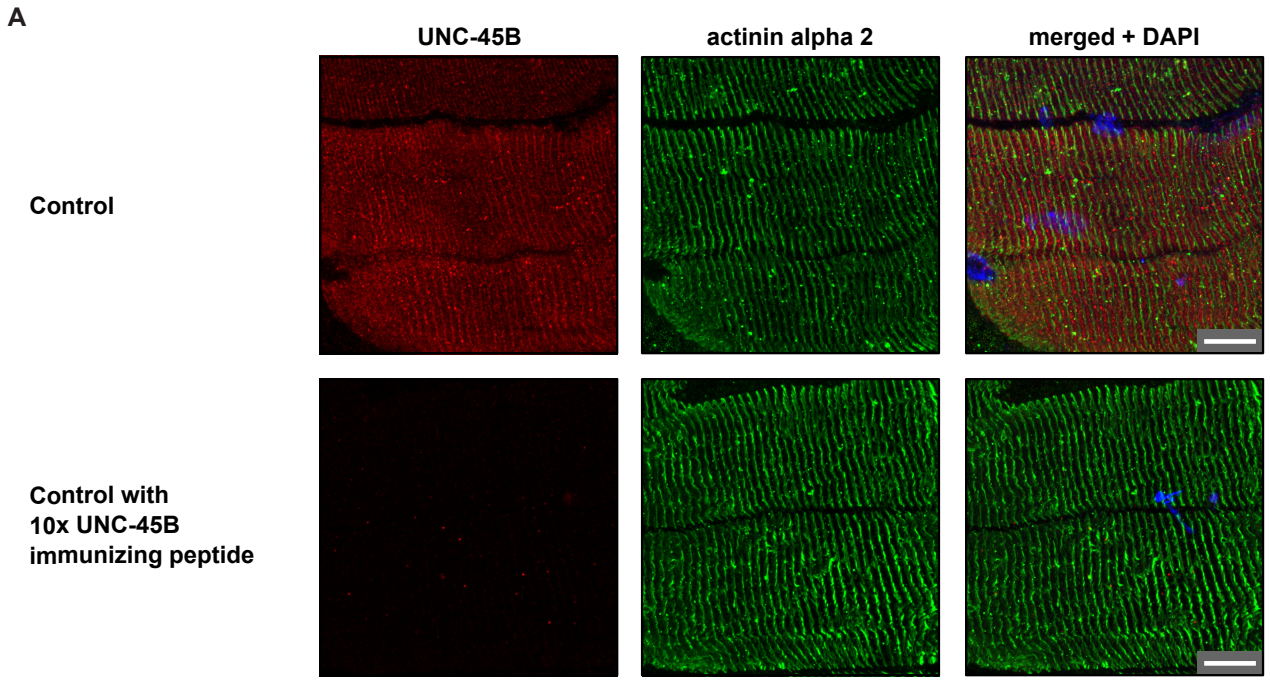
A
UNC-45B
actinin alpha 2
merged + DAPI
Control
Control with
10x UNC-45B
immunizing peptide

Figure S3

A

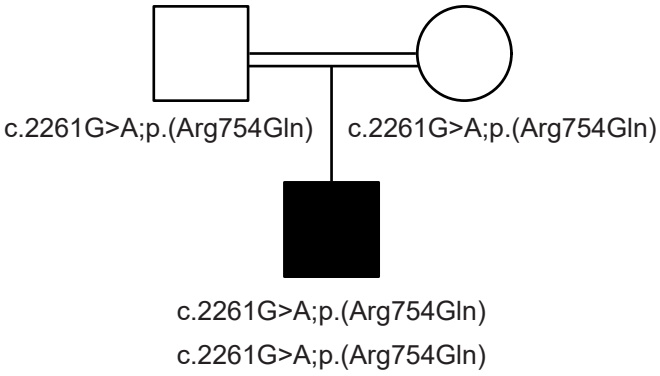

B

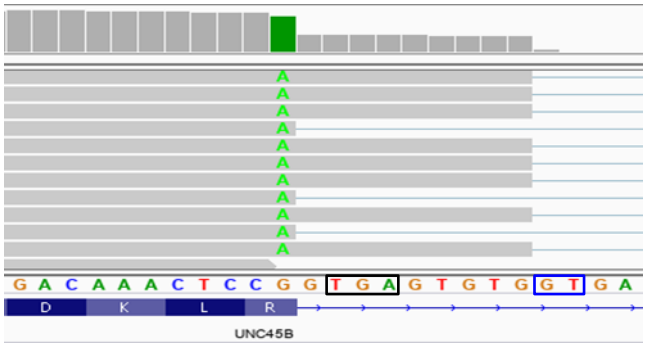

C

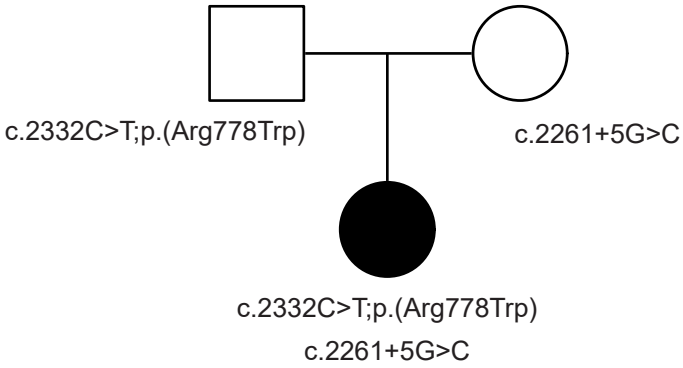

D

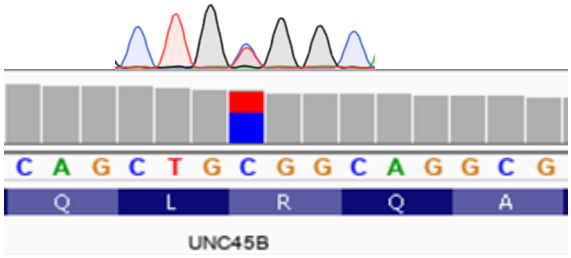

E

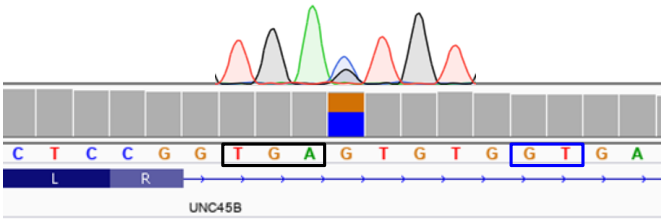

F

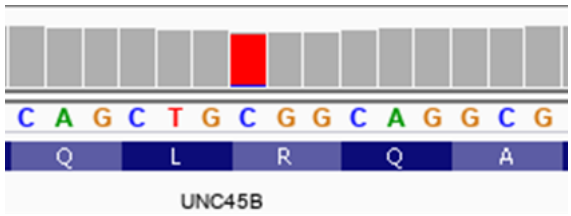

G

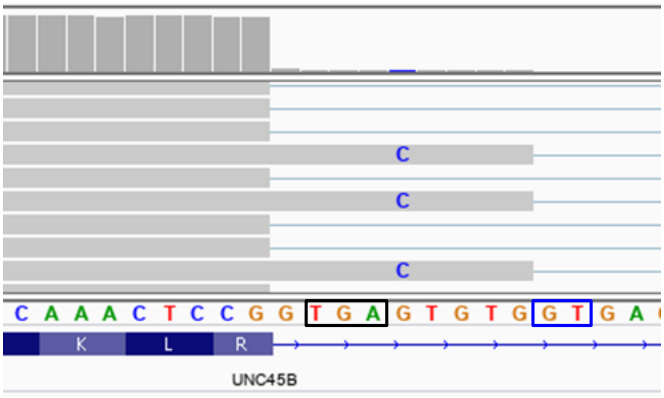

H

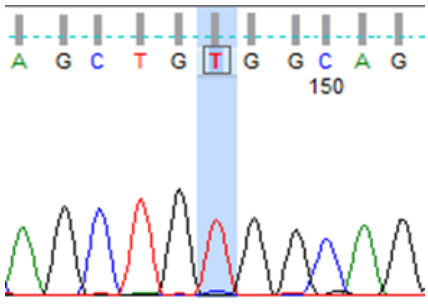

Figure S4

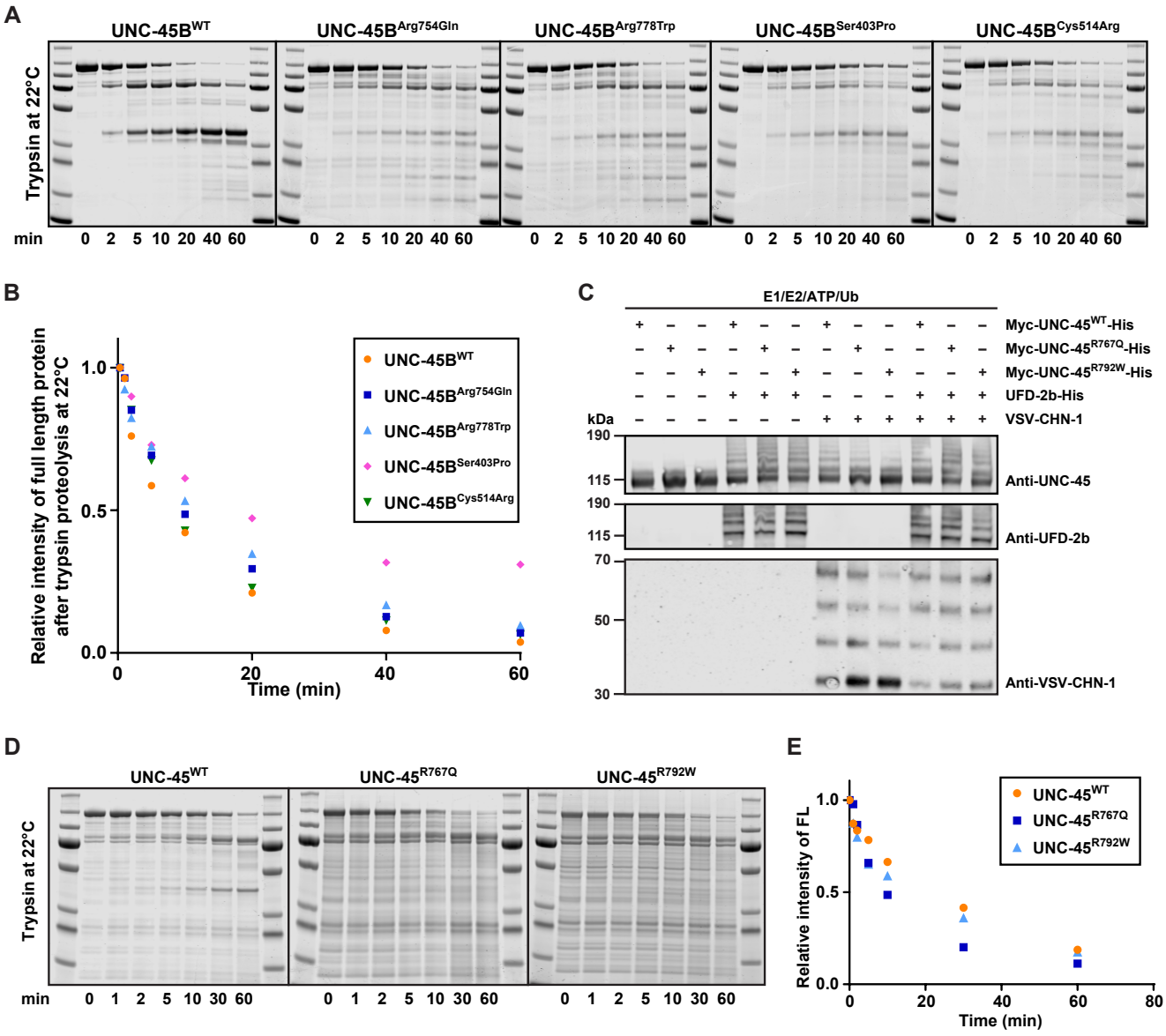
A
UNC-45B^WT
UNC-45B^Arg754Gln
UNC-45B^Arg778Trp
UNC-45B^Ser403Pro
UNC-45B^Cys514Arg
Trypsin at 22°C
min
0 2 5 10 20 40 60
B
Relative intensity of full length protein after trypsin proteolysis at 22°C
1.0
0.5
0.0
0
20
40
60
Time (min)
UNC-45B^WT
UNC-45B^Arg754Gln
UNC-45B^Arg778Trp
UNC-45B^Ser403Pro
UNC-45B^Cys514Arg
C
E1/E2/ATP/Ub
Myc-UNC-45^WT-His
Myc-UNC-45^R767Q-His
Myc-UNC-45^R792W-His
UFD-2b-His
VSV-CHN-1
kDa
190
115
70
50
30
Anti-UNC-45
Anti-UFD-2b
Anti-VSV-CHN-1
D
UNC-45^WT
UNC-45^R767Q
UNC-45^R792W
Trypsin at 22°C
min
0 1 2 5 10 30 60
E
Relative intensity of FL
1.0
0.5
0.0
0
20
40
60
80
Time (min)
UNC-45^WT
UNC-45^R767Q
UNC-45^R792W

Supplemental Figure Legends

Figure S1. Normal fiber contractile performance in P1 UNC-45B muscle. Muscle fiber contractile property from P1 (homozygous c.2261G>A *UNC45B*) was compared to controls. (A) Maximal tension generated by P1 fibers was similar to controls. (B) The calcium sensitivity of force was normal in P1 muscle compared to control. (C) Actin-myosin cross bridge attachment rates (K_{tr}) were normal in P1 muscle compared to type I control fibers, (D) with normal tension costs. Each data point in control bars represents the average of 8–15 muscle fibers from one control subject; each data point in P1 bar is one muscle fiber.

Figure S2. UNC-45B antibody is specific for the UNC-45B protein. (A) Longitudinal sections of control muscle biopsy incubated with either no UNC-45B immunizing peptide (top) or 10x excess of UNC-45B immunizing peptide (bottom), and stained for UNC-45B (red) and Z-disk protein α-actinin (green) confirmed the specificity of the UNC-45B antibody for the UNC-45B protein. Scale bar corresponds to 10 μm.

Figure S3. *UNC45B* pathogenic variants identified by exome sequencing. (A) Pedigree of P3. (B) BAM files visualized in Integrative Genomics Viewer (IGV) showing aligned P3 muscle RNA sequence reads from the homozygous c.2261G>A; p.(Arg754Gln) *UNC45B* variant. (C) Pedigree of P2. (D) Sanger Sequencing on P2 genomic DNA showing the c.2332C>T; p.(Arg778Trp) *UNC45B* variant (top) and BAM files visualized in Integrative Genomics Viewer (IGV) showing aligned sequence reads (bottom). (E) Sanger Sequencing on P2 genomic DNA showing the c.2261+5G>C

UNC45B variant (top) and BAM files visualized in IGV showing aligned sequence reads (bottom). (F) BAM files visualized in IGV showing aligned P2 muscle RNA sequence reads at the c.2332C>T; p.(Arg778Trp) *UNC45B* variant and revealing allelic imbalance in favor of the p.(Arg778Trp) variant. (G) BAM files visualized in IGV showing aligned P2 muscle RNA sequence reads of the c.2261+5G>C *UNC45B* variant and revealing the activation of a nearby intronic cryptic donor site which elongates the splice product to include an in-frame STOP codon. (H) Sequencing of reverse transcribed mRNA showing allelic imbalance towards the p.(Arg778Trp) variant.

Figure S4. *In vitro* analysis of human UNC-45B mutant proteins and *C. elegans* UNC-45 orthologue proteins. (A) Purified UNC-45B^{WT}, UNC-45B^{Arg754Gln}, UNC-45B^{Arg778Trp}, UNC-45B^{Ser403Pro}, and UNC-45B^{Cys514Arg} buffered solutions were subjected to partial proteolysis with trypsin at room temperature (22°C) and samples were loaded on SDS-PAGE gels for separation. Coomassie-stained gels are shown. (B) Quantification of full-length protein (FL, ~109 kDa) compared to time point 0 at 22°C. Results of three experiments. (C) *In vitro* ubiquitylation of purified UNC-45 wild-type and mutant proteins with the combination of enzymes indicated. The reaction was terminated by addition of SDS-PAGE sample buffer and analyzed by western blotting against UNC-45, UFD-2 and VSV-tagged CHN-1. (D) Purified *C. elegans* UNC-45^{WT}, UNC-45^{Arg767Gln}, and UNC-45^{Arg792Trp} solutions were subjected to partial proteolysis with trypsin at room temperature and samples were loaded on SDS-PAGE gels for separation. Coomassie stained gels are shown. (E) Quantification of full-length protein (FL, 109 kDa) compared to time point 0. Results of three independent experiments.

Supplemental Tables

Table S1. *UNC45B* variants identified.

DNA variant	RNA variant	Protein variant	*C. elegans* orthologous proteins
c.1207T>C	na	p.(Ser403Pro)	p.(Ile422Pro)
c.1540T>C	na	p.(Cys514Arg)	p.(Cys532Arg)
c.2261G>A	r.[2261g>a,2261_2262ins2261+1_2261+9]	p.(Arg754Gln), p.(Arg754GlnfsTer2)	p.(Arg767Gln)
c.2261+5G>C	r.2261_2262ins2261+1_2261+9	p.(Arg754GlnfsTer2)	p.(Arg767Gln)
c.2332C>T	r.2232c>u	p.(Arg778Trp)	p.(Arg792Trp)

Table S2. Oligonucleotides used in this study.

Name	5‘-3‘ sequence	Source
UNC-45B cDNA into pET21a FOR	gaagatctgATGGCAGAGGTGGAAGCG	This study
UNC-45B cDNA into pET21a REV	tggtggtgAGACACTGGTTTAATGAAACCATAATCCAT	This study
UNC-45B cDNA into pET21a vector FOR	CAGTGTCTcaccaccaccaccaccacta	This study
UNC-45B cDNA into pET21a vector REV	CTCTGCCATcagatcttcttcagaaataagtttttgttcc	This study
UNC-45B Arg754Gln mutagenesis FOR	GACAAACTCCaGCAGAAGATCTTTAAGGAG	This study
UNC-45B Arg754Gln mutagenesis REV	ACTCCGCCCAGACAGGTT	This study
UNC-45B Arg778Trp mutagenesis FOR	TGATCAGCTGtGGCAGGCGGC	This study
UNC-45B Arg778Trp mutagenesis REV	TGATTCTCAAACATGTAGTTCTCGATGTCTGG	This study
UNC-45B Ser403Pro mutagenesis FOR	CCAGACAGTGcCAGGGATCCT	This study
UNC-45B Ser403Pro mutagenesis REV	ATGGCATTCAAGTTCTTGTC	This study
UNC-45B Cys514Arg mutagenesis FOR	GGCCAAACAGcGTCGCAAGTG	This study

Name	5‘-3‘ sequence	Source
UNC-45B Cys514Arg mutagenesis REV	AGTTTTTCTGTCGACCCTTC	This study
UNC-45 Arg767Gln mutagenesis FOR	GATTCGATTCagGGACGAATTTTGAAAGAGAAG	This study
UNC-45 Arg767Gln mutagenesis REV	ACTGACGCTTGCCAAGTT	This study
UNC-45 Arg792Trp mutagenesis FOR	CGAGCATTTGtggGCCGCCGCCG	This study
UNC-45 Arg792Trp mutagenesis REV	TGATCCGTCATAAACCAGAATTCCTCAATCTTTG	This study
UNC-45 Ile422Pro mutagenesis FOR	ATGCTTCTTGccTACAATGCTTCAAG	This study
UNC-45 Ile422Pro mutagenesis REV	GATAGTTTGATACGGTATTTG	This study
UNC-45 Cys532Arg mutagenesis FOR	GGCGAAGACTcGCAAGAAATTC	This study
UNC-45 Cys532Arg mutagenesis REV	AAACTGATCACTGCTTCTTC	This study
unc-45 genotyping FOR	AGATCAAGGCGGGACATGC	This study
unc-45(m94) genotyping REV in combination with EcoRI digestion	TCCACTCGATACTTGTTCGCTTTCT	This study
FLAG-tag genotyping REV in combination with BsmFI digestion for R767Q substitution or in combination with Sau96I digestion for R792W substitution	GTCATCGTCATCCTTGTAATC	This study

Table S3. *C. elegans* strains used in this study.

Strain name	Origin	Resource
C. elegans: Bristol (N2) strain as wild type (WT)	CGC	Wormbase ID: N2
unc-119(ed4)III	Baumeister Lab	BR854
unc-45(m94)III	CGC	Wormbase ID: DR94
unc-45(m94)III; hhIs84[unc-119(+); unc-54::unc-45^{FLAG}]	Hoppe Lab	Gazda et al., 2013
unc-45(m94)III; hhIs238[unc-119(+); unc-54::unc-45R767Q^{FLAG}]	this study	N/A
unc-45(m94)III; hhIs243[unc-119(+); unc-54::unc-45R792W^{FLAG}]	this study	N/A
unc-45(m94)III; hhIs254[unc-119(+); Punc-54::unc-45I422P^{FLAG}]	this study	N/A
unc-45(m94)III; hhIs253[unc-119(+); Punc-54::unc-45C532R^{FLAG}]	this study	N/A

Table S4. Relative fluorescence signal in partial trypsin proteolysis of recombinant UNC-45B mutant proteins at 37°C.

Time (min)	UNC-45B(WT)			
	1	2	MEAN	SD
0	1.00	1.00	1.00	0.00
1		0.88	0.88	
2	0.65	0.68	0.66	0.02
5	0.22	0.29	0.25	0.05
10	0.05	0.08	0.06	0.02
20	0.01	0.03	0.02	0.01
40	0.01	0.01	0.01	0.00
60	0.01	0.01	0.01	0.00

Time (min)	UNC-45B(Arg754Gln)				UNC-45B(Arg778Trp)			
	1	2	MEAN	SD	1	2	MEAN	SD
0	1.00	1.00	1.00	0.00	1.00	1.00	1.00	0.00
1		0.90	0.90			0.83	0.83	
2	0.68	0.74	0.71	0.04	0.62	0.70	0.66	0.06
5	0.32	0.48	0.40	0.11	0.32	0.40	0.36	0.05
10	0.20	0.34	0.27	0.09	0.20	0.31	0.26	0.08
20	0.19	0.28	0.24	0.07	0.13	0.24	0.19	0.08
40	0.15	0.25	0.20	0.07	0.15	0.13	0.14	0.02
60	0.12	0.10	0.11	0.01	0.08	0.25	0.17	0.12

Time (min)	UNC-45B(Ser403Pro)				UNC-45B(Cys514Arg)			
	1	2	MEAN	SD	1	2	MEAN	SD
0	1.00	1.00	1.00	0.00	1.00	1.00	1.00	0.00
1		0.98	0.98			0.93	0.93	
2	0.95	0.88	0.91	0.05	0.66	0.82	0.74	0.11
5	0.60	0.60	0.60	0.00	0.33	0.60	0.47	0.19
10	0.43	0.54	0.48	0.08	0.18	0.37	0.28	0.13
20	0.45	0.35	0.40	0.07	0.13	0.30	0.22	0.12
40	0.09	0.34	0.21	0.17	0.11	0.23	0.17	0.08
60	0.08	0.31	0.20	0.16	0.11	0.15	0.13	0.03

Table S5. Parameters of Boltzmann sigmoidal curve fit to normalized SYPRO fluorescence signals in thermal shift assay of recombinant UNC-45B mutant proteins.

	UNC45B^{WT}	UNC45B^{R754Q}	UNC45B^{R778W}	UNC45B^{S403P}	UNC45B^{C514R}
Boltzmann sigmoidal					
Best-fit values					
Bottom	= 0	= 0	= 0	= 0	= 0
Top	= 1	= 1	= 1	= 1	= 1
V50	43.16	38.18	37.85	37.88	36.9
Slope	1.58	1.324	1.464	1.274	1.742
Std. Error					
V50	0.04358	0.05145	0.04907	0.1241	0.03901
Slope	0.03976	0.04617	0.04361	0.1148	0.03492
95% CI (profile likelihood)					
V50	43.07 to 43.25	38.08 to 38.28	37.75 to 37.94	37.63 to 38.13	36.83 to 36.98
Slope	1.502 to 1.66	1.235 to 1.417	1.38 to 1.552	1.061 to 1.518	1.675 to 1.81
Goodness of Fit					
Degrees of Freedom	86	60	76	48	81
R square	0.9903	0.9852	0.9887	0.9061	0.9936
Absolute Sum of Squares	0.1025	0.1196	0.1248	0.5738	0.07059
Sy.x	0.03452	0.04465	0.04053	0.1093	0.02952
Constraints					
Bottom	Bottom = 0	Bottom = 0	Bottom = 0	Bottom = 0	Bottom = 0
Top	Top = 1	Top = 1	Top = 1	Top = 1	Top = 1
Number of points					
# of X values	123	123	123	114	123
# Y values analyzed	88	62	78	50	83

Table S6. Single normalized fluorescence values of thermal shift assays of recombinant UNC-45B mutant proteins.

Temperature (°C)	UNC-45B(WT)					UNC-45B(Arg754Gln)					UNC-45B(Arg778Trp)				
Replicate:	1	2	3	MEAN	SD	1	2	3	MEAN	SD	1	2	3	MEAN	SD
30.0															
30.5															
31.0											0.000000	0.032292	0.000000	0.010764	0.018644
31.5			0.000000	0.000000							0.000829	0.048511	0.000513	0.016618	0.027621
32.0			0.000104	0.000104							0.004261	0.065842	0.002395	0.024166	0.036105
32.5			0.000449	0.000449							0.010298	0.084136	0.005713	0.033382	0.044013
33.0			0.001122	0.001122							0.019768	0.103466	0.010571	0.044602	0.051185
33.5	0		0.002279	0.001140	0.001612	0.000000	0.084682	0.000000	0.028227	0.048891	0.034209	0.123759	0.017618	0.058529	0.057097
34.0	0.000896		0.004006	0.002451	0.002199	0.006790	0.105336	0.003368	0.038498	0.057909	0.055990	0.145756	0.028188	0.076645	0.061445
34.5	0.002740		0.006475	0.004608	0.002641	0.023173	0.128830	0.012009	0.054671	0.064466	0.086056	0.170197	0.044267	0.100173	0.064141
35.0	0.006060	0.000000	0.009842	0.005301	0.004965	0.052546	0.156110	0.028937	0.079198	0.067646	0.126776	0.198341	0.068555	0.131224	0.065007
35.5	0.011118	0.001725	0.014332	0.009058	0.006551	0.096974	0.189415	0.057609	0.114666	0.067661	0.179096	0.232780	0.103790	0.171889	0.064796
36.0	0.018021	0.005174	0.020065	0.014420	0.008072	0.157491	0.230120	0.100727	0.162779	0.064859	0.243016	0.274922	0.152094	0.223344	0.063734
36.5	0.026979	0.010693	0.027265	0.021646	0.009486	0.233210	0.279690	0.159532	0.224144	0.060590	0.316170	0.326915	0.213875	0.285653	0.062393
37.0	0.038360	0.018455	0.036089	0.030968	0.010896	0.322066	0.338296	0.233138	0.297834	0.056612	0.397254	0.387794	0.287630	0.357559	0.060745
37.5	0.052482	0.029148	0.046829	0.042820	0.012173	0.419336	0.404647	0.318488	0.380824	0.054482	0.482244	0.457117	0.370177	0.436513	0.058807
38.0	0.069396	0.042946	0.059641	0.057328	0.013376	0.519705	0.477022	0.410529	0.469085	0.055019	0.567708	0.531847	0.456794	0.518783	0.056599
38.5	0.089525	0.060021	0.074923	0.074823	0.014752	0.617565	0.551549	0.504387	0.557834	0.056850	0.650095	0.607984	0.543069	0.600383	0.053916
39.0	0.113394	0.080890	0.093053	0.095779	0.016423	0.708635	0.625301	0.595409	0.643115	0.058677	0.725852	0.682566	0.625103	0.677840	0.050541
39.5	0.141216	0.105381	0.114465	0.120354	0.018629	0.789225	0.695009	0.679695	0.721310	0.059313	0.793561	0.751666	0.700021	0.748416	0.046855
40.0	0.173464	0.134357	0.139761	0.149194	0.021191	0.857122	0.758348	0.754719	0.790063	0.058103	0.851089	0.813509	0.766112	0.810237	0.042583
40.5	0.210349	0.167989	0.169444	0.182594	0.024047	0.910849	0.814114	0.819729	0.848230	0.054302	0.897846	0.866390	0.823105	0.862447	0.037526
41.0	0.252556	0.206968	0.204289	0.221271	0.027126	0.951144	0.861618	0.873837	0.895533	0.048547	0.934422	0.909717	0.870895	0.905011	0.032024
41.5	0.300295	0.252328	0.244919	0.265848	0.030062	0.978745	0.901377	0.917531	0.932551	0.040813	0.962003	0.944156	0.909996	0.938718	0.026426
42.0	0.354042	0.305105	0.292197	0.317115	0.032624	0.994539	0.933735	0.951520	0.959931	0.031262	0.981297	0.970004	0.941502	0.964268	0.020508
42.5	0.414006	0.366161	0.346623	0.375597	0.034668	1.000000	0.959639	0.976336	0.978658	0.020281	0.993726	0.987409	0.966030	0.982389	0.014515
43.0	0.480135	0.436357	0.408717	0.441736	0.036012		0.979518	0.992378	0.985948	0.009093	1.000000	0.997408	0.983990	0.993799	0.008593
43.5	0.551691	0.514660	0.478200	0.514851	0.036746		0.993115	1.000000	0.996558	0.004868		1.000000	0.995519	0.997759	0.003169
44.0	0.627305	0.600207	0.553848	0.593787	0.037147		1.000000		1.000000				1.000000	1.000000	
44.5	0.704447	0.690238	0.633329	0.676005	0.037635										
45.0	0.779640	0.779062	0.713639	0.757447	0.037940										
45.5	0.849194	0.861676	0.790703	0.833858	0.037891										
46.0	0.909105	0.930666	0.860256	0.900009	0.036076										
46.5	0.955949	0.978786	0.918309	0.951014	0.030539										
47.0	0.986721	1.000000	0.961995	0.982905	0.019288										
47.5	1.000000		0.989432	0.994716	0.007472										
48.0			1.000000	1.000000											

Temperature (°C)	UNC-45B(Ser403Pro)					UNC-45B(Cys514Arg)				
Replicate:	1	2	3	MEAN	SD	1	2	3	MEAN	SD
30.0						0.000000	0.000000	0.000000	0.000000	0.000000
30.5						0.009974	0.016816	0.011468	0.012753	0.003598
31.0						0.022260	0.035468	0.024631	0.027453	0.007041
31.5						0.037123	0.056014	0.039488	0.044208	0.010292
32.0						0.055023	0.079129	0.056525	0.063559	0.013505
32.5						0.076161	0.105241	0.075939	0.085780	0.016854
33.0						0.100799	0.134043	0.098193	0.111012	0.019988
33.5	0.000000			0.000000		0.129797	0.166391	0.124254	0.140148	0.022896
34.0	0.003481			0.003481		0.164344	0.203265	0.154960	0.174190	0.025614
34.5	0.017108	0.242701	0.000000	0.086603	0.135455	0.204901	0.245093	0.190971	0.213655	0.028103
35.0	0.045554	0.277828	0.009984	0.111122	0.145463	0.252527	0.292546	0.233057	0.259376	0.030330
35.5	0.090113	0.319343	0.032158	0.147205	0.151866	0.307418	0.346848	0.281482	0.311916	0.032914
36.0	0.151482	0.368157	0.068011	0.195883	0.154921	0.368584	0.406959	0.335652	0.370398	0.035688
36.5	0.228367	0.429288	0.118128	0.258594	0.157767	0.434705	0.471901	0.394576	0.433728	0.038672
37.0	0.318679	0.499544	0.182054	0.333426	0.159258	0.504128	0.539779	0.457001	0.500303	0.041521
37.5	0.418938	0.577099	0.258688	0.418241	0.159207	0.574609	0.608573	0.521406	0.568196	0.043936
38.0	0.524070	0.659215	0.344852	0.509379	0.157696	0.643636	0.676512	0.585900	0.635349	0.045871
38.5	0.628804	0.740876	0.437500	0.602393	0.153403	0.709690	0.740659	0.649006	0.699785	0.046622
39.0	0.727770	0.816606	0.533001	0.692459	0.145063	0.770791	0.800220	0.709295	0.760102	0.046395
39.5	0.817088	0.883212	0.627140	0.775813	0.132932	0.825748	0.852871	0.765314	0.814645	0.044822
40.0	0.891387	0.937044	0.715573	0.848001	0.116936	0.873241	0.897695	0.815919	0.862285	0.041975
40.5	0.946588	0.974453	0.795449	0.905497	0.096317	0.912676	0.934385	0.860470	0.902510	0.037992
41.0	0.982693	0.995894	0.863978	0.947522	0.072651	0.943788	0.962453	0.898351	0.934864	0.032970
41.5	1.000000	1.000000	0.918957	0.972986	0.046790	0.967105	0.982633	0.929431	0.959723	0.027358
42.0			0.959803	0.959803		0.983222	0.994802	0.954238	0.977421	0.020895
42.5			0.986644	0.986644		0.993328	1.000000	0.973080	0.988803	0.014019
43.0			1.000000	1.000000		0.998679		0.986661	0.992670	0.008498
43.5						1.000000		0.995620	0.997810	0.003097
44.0								1.000000	1.000000	
44.5										
45.0										
45.5										
46.0										
46.5										
47.0										
47.5										
48.0										

Supplemental Methods

Whole Exome Sequencing

Trio WES for P1 and singleton WES for P5 was performed at the Broad Institute (Boston, USA) using Standard Germline Exome version 5, handled by the Genomics Platform's Core Exome/RNA product team. The process includes sample prep (Illumina Nextera), hybrid capture (Illumina Rapid Capture Enrichment 37Mb target), sequencing (Illumina, 150bp paired reads) and identification quality control check. The hybrid selection libraries typically meet or exceed 85% of targets at 20x, comparable to ~55x mean coverage.

Trio WES for P2 was performed using the SureSelect Human All Exon 50Mb capture library v5 (Agilent, Santa Clara, USA) and paired-end sequencing on Illumina HiSeq2500 (Illumina, San Diego, USA) with 30X coverage. The data were aligned to the GRCh37/hg19 reference genome, and variants were filtered according to their frequency in gnomAD (http://gnomad.broadinstitute.org/).

WES for P3 and P4 was performed using Nextera Flex for Enrichment library preparation (Illumina, San Diego, CA, USA). Libraries were sequenced using a NextSeq500 sequencer (Illumina, San Diego, CA, USA) with 150 bp paired-end reads. The reads were mapped to the human reference genome (GRCh37/hg19) by Burrows–Wheeler Aligner (BWA) bwa v0.7.17. Duplicate reads were removed with picard v2.2. On average, for P3 mean depth was 119X with 94.33% of regions covered at least 20X. For P4 mean depth was 101X with 93.5% of regions covered at least 20x. Variant calling was realized using the Genome Analysis Toolkit (GATK) v4.0.7.0 and annotated with Varaft 2V.16 [1].

WES for P6, P7 and P8 was performed using SureSelectXT Human All Exon V6 (Agilent Technologies, Santa Clara, CA, USA). Captured DNA was sequenced using a HiSeq 1000 (Illumina, San Diego, CA, USA) with 150 bp paired-end reads. The reads were mapped to the human reference genome (GRCh37/hg19) by Burrows–Wheeler Aligner (BWA) 0.7.5a-r405. Duplicate reads were removed with Picard 1.99. Variants were identified with the Genome Analysis Toolkit (GATK) v3.2 based on the GATK Best Practice Workflow and annotated with ANNOVAR (2017Jul16).

WES for P9 was performed as described elsewhere[2]. Briefly, target enrichment was performed with 2 µg genomic DNA using the SureSelectXT Human All Exon Kit V6 (Agilent Technologies, Santa Clara, CA, USA) to generate barcoded whole-exome sequencing libraries. Libraries were sequenced on the HiSeqX platform (Illumina, San Diego, CA, USA) with 50x coverage. Quality assessment of the sequence reads was performed by generating QC statistics with FastQC (http://www.bioinformatics.bbsrc.ac.uk/projects/fastqc). The bioinformatics filtering strategy included screening for only exonic and donor/acceptor splicing variants. In accordance with the pedigree and phenotype, priority was given to rare variants (<0.01% in public databases, including 1,000 Genomes project, NHLBI Exome Variant Server, Complete Genomics 69, and Exome Aggregation Consortium [ExAC v0.2]) that were fitting a recessive (homozygous or compound heterozygous) or a de novo model and/or variants in genes previously linked to proximal myopathy and other neurological disorders.

WES for P10 was performed by target enrichment on genomic DNA using the SureSelectXT Human All Exon V6 (Agilent Technologies, Santa Clara, CA, USA) and the

HiSeq2500 platform for sequencing (Illumina, San Diego, CA, USA). The paired-end reads were aligned to the reference genome (GRCh37/hg19) using the CLC Biomedical Genomics workbench (Qiagen, Hilden, Germany). On average, 90% of all regions were covered at least 7x. Data were analyzed using Ingenuity Variant Analysis (IVA) (Qiagen, Hilden, Germany).

Confirmation of variants and segregation was performed by Sanger sequencing.

RNA Sequencing

For P2, P3 and P4 muscle lysates were prepared with a Precellys 24 homogenizer (Bertin, Montigny-le-Bretonneux, France). RNA isolation and purification were performed using the TRI Reagent (MRC, Mongomery, USA), and paired-end sequenced on Illumina HiSeq2500 (Illumina, San Diego, USA). The data were aligned to the GRch38 reference genome. For splicing verifications, cDNA synthesis was performed with the SuperScript IV RT (Thermofischer, Waltham, USA) and amplified with *UNC45B*-specific primers.

Permeabilized muscle fiber mechanics

Single fibers were dissected from the muscle biopsies and permeabilized overnight as described previously[3]. This procedure renders the membranous structures in the muscle fibers permeable, which enables activation of the myofilaments with exogenous calcium. Preparations were washed thoroughly with relaxing solution and stored in 50% glycerol/relaxing solution at −20 °C. Single muscle fibers were dissected from the permeabilized strips, and were mounted using aluminum T-clips between a length motor (ASI 315C-I, Aurora Scientific Inc., Ontario, Canada) and a force transducer element (ASI

403A, Aurora Scientific Inc., Ontario, Canada) in a single fiber apparatus (ASI 802D, Aurora Scientific Inc., Ontario, Canada) that was mounted on the stage of an inverted microscope (Zeiss Axio Observer A1). Sarcomere length was determined using a high speed VSL camera and ASI 900B software (Aurora Scientific Inc., Ontario, Canada). Mechanical experiments were performed at a sarcomere length of 2.5 µm, to ensure that the sarcomeres operate at an optimal length (middle of the plateau phase). Fiber width and diameter were measured at three points along the fiber and the cross-sectional area was determined assuming an elliptical cross-section. The bathing solutions used during the experimental protocols were: a relaxing solution (100 mM BES, 6.97 mM EGTA, 6.48 mM $MgCl_2$, 5.89 mM Na_2-ATP, 40.76 mM K-propionate, 14.5 mM creatine phosphate), a pre-activating solution with low EGTA concentration (100 mM BES, 0.1 mM EGTA, 6.42 mM $MgCl_2$, 5.87 mM Na_2-ATP, 41.14 mM K-propionate, 14.5 mM creatine phosphate, 6.9 mM HDTA), and an activating solution (100 mM BES, 7.0 mM Ca-EGTA, 6.28 mM $MgCl_2$, 5.97 mM Na_2-ATP, 40.64 mM K-propionate, 14.5 mM creatine phosphate). The temperature of the bathing solutions was kept constant at 20°C using a TEC controller (ASI 825A, Aurora Scientific Inc. Ontario, Canada). The relaxation kinetics were calculated by fitting a mono-exponential through the force relaxation curve. To investigate the sarcomere-length dependency of force, maximal active tension was measured at incremental sarcomere lengths (2.0 – 3.5 µm).

To investigate submaximal force generating capacities at the sarcomere level, force-pCa relations were established. To determine the force-pCa relation (pCa = -log of molar free Ca^{2+} concentration), permeabilized muscle fibers were sequentially bathed in solutions with pCa values ranging from 4.5 to 9.0 and the steady-state force was measured. Force values were normalized to the maximal force obtained at pCa 4.5. The

obtained force-pCa data were fit to the Hill equation, providing the pCa_{50} and the Hill coefficient, n_H, an index of myofilament cooperativity.

To assess the tension cost during contraction, ATPase activity (temperature 12°C) at saturating [Ca^{2+}] (pCa 4.5) was measured photometrically by enzymatic coupling of the regeneration of ATP to the oxidation of NADH present in the bathing solution[4]. Sarcomere length was set at 2.5 µm. NADH breakdown was monitored via the absorption of near UV light at 340 nm. The activation buffer contained 10 mm phosphoenol pyruvate, with 4 mg•ml^{-1} pyruvate kinase (500 U•mg^{-1}), 0.24 mg•ml^{-1} lactate dehydrogenase (870 U•mg^{-1}) and 20 µm diadenosine-5′ pentaphosphate (A_2P_5). Briefly, the set up consisted of two anodized aluminium troughs (volume 80 µl each) containing relaxing and pre-activating solution and a measuring chamber (volume about 30 µl) containing activating solution. The solution was continuously stirred via a membrane at the base of the chamber. UV light passed through the chamber beneath the fibre, and the transmitted light was monitored by two UV-enhanced photodiodes at 340 and 400 nm. The photodiode at 400 nm provided a reference signal, independent of NADH concentration. A syringe, controlled by a stepper motor, was used to add 0.05 µl of 10 mM ADP at the end of each recording to calibrate the absorbance signal. Force during the enzymatic assay was measured by means of a strain gauge transducer (AE801 SensoNor, Horten, Norway). The force and the absorbance signals were filtered at 1 kHz and 2.5 Hz, respectively. The ATPase rate was measured as the slope over time of the absorbance signal. The ATPase rate was divided by tension (force/CSA) to determine the tension cost.

As the contractile properties of muscle fibers are influenced by the myosin heavy chain composition of the muscle fibers, we used a specialized SDS-PAGE technique to analyze the myosin heavy chain isoform composition in the muscle fibers used in

contractility experiments. In brief, muscle fibers were denatured by boiling for 2 minutes in SDS sample buffer. The stacking gel contained a 4% acrylamide concentration (pH 6.7), and the separating gel contained 7% acrylamide (pH 8.7) with 30% glycerol (v/v). The gels were run for 24h at 15 °C and a constant voltage of 275 volt. Finally, the gels were silver-stained, scanned, and analyzed with ImageQuant TL software (GE Healthcare, Chicago, IL).

Immunostaining & microscopy

Pre-cooled 100% methanol fixed 8 μm muscle longitudinal sections were blocked in PBS with 10% goat serum and 0.1% Tx-100, then incubated with primary antibodies anti-UNC-45B (HPA017861, Sigma) and anti-α-Actinin (A7811,sigma) with 10x of PrEST Antigen UNC-45B (APREST72666, Sigma) at 4°C overnight. The antibody labeling was detected with secondary antibodies Alexa 488- conjugated goat anti-mouse IgG and Alexa 568-conjugated goat anti-rabbit IgG (Thermofisher, Rockford, IL) for 1h at room temperature. Prepared muscle sections were imaged with a Zeiss Airy microscope (Zeiss, Germany).

In vitro ubiquitylation assay

Briefly, *C. elegans* UNC-45 recombinant proteins were incubated with *C. elegans* CHN-1 and UFD-2b recombinant proteins and the extent of ubiquitylation was evaluated in a western blot. Reactions were done in ubiquitinylation buffer (Enzo), supplemented with 1x ATP Regeneration Buffer (Enzo) and 50 μM ubiquitin (Flag-tagged, Boston Biochem). Ubiquitin activating enzyme E1 (His-tagged, Enzo) was used at a concentration of 0.1 μM. Enzyme E2 (LET-70-6xHIS), VSV-CHN-1-6xHIS and UFD-2b-6xHIS were purified in-house via HIS-binding to HisTrap FF columns on an ÄKTApurifier (GE Healthcare) or to

Ni-NTA agarose (QIAGEN). E2, E3 and substrate proteins were used at a concentration of 0.2 µM. After incubation at 30°C for 2 h, reactions were stopped by addition of 2x SDS-PAGE sample buffer (125 mM Tris pH 6.8, 4 % SDS, 20 % glycerol, 0.03 % bromophenol blue, 0.05 % β-mercaptoethanol) and boiling at 95°C for 5 min. Samples were run on 4-12% Bis-Tris gels (Invitrogen), transferred to nitrocellulose membranes, probed with antibodies for *C. elegans* UNC-45, UFD-2b (Biogenes) and VSV-tagged CHN-1 (P5D4, Roche), and detected using IRDye@ 800CW Goat anti-Mouse IgG secondary antibodies (LI-COR Biotechnology) on an Odyssey CLx Imager (LI-COR Biotechnology).

References

1. Desvignes, J.P., Bartoli, M., Delague, V., Krahn, M., Miltgen, M., Beroud, C., and Salgado, D. (2018). VarAFT: a variant annotation and filtration system for human next generation sequencing data. Nucleic Acids Res 46, W545-W553.
2. Mencacci, N.E., Kamsteeg, E.J., Nakashima, K., R'Bibo, L., Lynch, D.S., Balint, B., Willemsen, M.A., Adams, M.E., Wiethoff, S., Suzuki, K., et al. (2016). De Novo Mutations in PDE10A Cause Childhood-Onset Chorea with Bilateral Striatal Lesions. Am J Hum Genet 98, 763-771.
3. de Winter, J.M., Molenaar, J.P., Yuen, M., van der Pijl, R., Shen, S., Conijn, S., van de Locht, M., Willigenburg, M., Bogaards, S.J., van Kleef, E.S., et al. (2020). KBTBD13 is an actin-binding protein that modulates muscle kinetics. The Journal of clinical investigation 130, 754-767.
4. Ottenheijm, C.A., Lawlor, M.W., Stienen, G.J., Granzier, H., and Beggs, A.H. (2011). Changes in cross-bridge cycling underlie muscle weakness in patients with tropomyosin 3-based myopathy. Hum Mol Genet 20, 2015-2025.

Supplemental Acknowledgements

This research was supported (in part) by the Intramural Research Program of the NIH, NINDS to CGB and by the Deutsche Forschungsgemeinschaft (DFG) (FOR2743 and CECAD) to TH, DFG (FOR2743) and the European Molecular Biology Organization (EMBO) (Installation Grant No. 3916) to WP. Sequencing and analysis were provided by the Broad Institute of MIT and Harvard Center for Mendelian Genomics (Broad CMG) and was funded by the National Human Genome Research Institute,

the National Eye Institute, and the National Heart, Lung and Blood Institute grant UM1 HG008900 and in part by National Human Genome Research Institute grant R01 HG009141. Family P9 was collected as part of the SYNaPS Study Group collaboration funded by The Wellcome Trust and strategic award (Synaptopathies) funding (WT093205 MA and WT104033AIA). This research was conducted as part of the Queen Square Genomics group at University College London, supported by the National Institute for Health Research University College London Hospitals Biomedical Research Centre. This study was partially supported by the Intramural Research Grant (29-4 to NI; 30-9 to SN, AI) for Neurological and Psychiatric Disorders of NCNP; and by AMED under Grant Numbers JP19ek0109285h0003 and Joint Usage and Joint Research Programs, the Institute of Advanced Medical Sciences, Tokushima University (2019, A9 to AI). This work was supported by the Association Belge contre les Maladies Neuromusculaire (ABMM) and the EU Horizon 2020 program (Solve-RD). JB is supported by a Senior Clinical Researcher mandate of the Research Fund - Flanders (FWO). Authors of this publication are member of the European Reference Network for Rare Neuromuscular Diseases (ERN EURO-NMD) and of the European Reference Network for Rare Neurological Diseases (ERN-RND).This work was supported by the France Génomique National infrastructure, funded as part of the «Investissements d'Avenir» program managed by the Agence Nationale pour la Recherche (ANR-10-INBS-09), and by Fondation Maladies Rares within the frame of the "Myocapture" sequencing project.